Time-dependent and time-integrated angular analysis of $B \to \varphi K^0_S \pi^0$ and $\varphi K^\pm \pi^\mp$

B. Aubert,[1] M. Bona,[1] Y. Karyotakis,[1] J. P. Lees,[1] V. Poireau,[1] E. Prencipe,[1] X. Prudent,[1] V. Tisserand,[1] J. Garra Tico,[2] E. Grauges,[2] L. Lopez,[3a,3b] A. Palano,[3a,3b] M. Pappagallo,[3a,3b] G. Eigen,[4] B. Stugu,[4] L. Sun,[4] G. S. Abrams,[5] M. Battaglia,[5] D. N. Brown,[5] R. N. Cahn,[5] R. G. Jacobsen,[5] L. T. Kerth,[5] Yu. G. Kolomensky,[5] G. Lynch,[5] I. L. Osipenkov,[5] M. T. Ronan,[5,*] K. Tackmann,[5] T. Tanabe,[5] C. M. Hawkes,[6] N. Soni,[6] A. T. Watson,[6] H. Koch,[7] T. Schroeder,[7] D. Walker,[8] D. J. Asgeirsson,[9] B. G. Fulsom,[9] C. Hearty,[9] T. S. Mattison,[9] J. A. McKenna,[9] M. Barrett,[10] A. Khan,[10] V. E. Blinov,[11] A. D. Bukin,[11] A. R. Buzykaev,[11] V. P. Druzhinin,[11] V. B. Golubev,[11] A. P. Onuchin,[11] S. I. Serednyakov,[11] Yu. I. Skovpen,[11] E. P. Solodov,[11] K. Yu. Todyshev,[11] M. Bondioli,[12] S. Curry,[12] I. Eschrich,[12] D. Kirkby,[12] A. J. Lankford,[12] P. Lund,[12] M. Mandelkern,[12] E. C. Martin,[12] D. P. Stoker,[12] S. Abachi,[13] C. Buchanan,[13] J. W. Gary,[14] F. Liu,[14] O. Long,[14] B. C. Shen,[14,*] G. M. Vitug,[14] Z. Yasin,[14] L. Zhang,[14] V. Sharma,[15] C. Campagnari,[16] T. M. Hong,[16] D. Kovalskyi,[16] M. A. Mazur,[16] J. D. Richman,[16] T. W. Beck,[17] A. M. Eisner,[17] C. J. Flacco,[17] C. A. Heusch,[17] J. Kroseberg,[17] W. S. Lockman,[17] A. J. Martinez,[17] T. Schalk,[17] B. A. Schumm,[17] A. Seiden,[17] M. G. Wilson,[17] L. O. Winstrom,[17] C. H. Cheng,[18] D. A. Doll,[18] B. Echenard,[18] F. Fang,[18] D. G. Hitlin,[18] I. Narsky,[18] T. Piatenko,[18] F. C. Porter,[18] R. Andreassen,[19] G. Mancinelli,[19] B. T. Meadows,[19] K. Mishra,[19] M. D. Sokoloff,[19] P. C. Bloom,[20] W. T. Ford,[20] A. Gaz,[20] J. F. Hirschauer,[20] M. Nagel,[20] U. Nauenberg,[20] J. G. Smith,[20] K. A. Ulmer,[20] S. R. Wagner,[20] R. Ayad,[21,†] A. Soffer,[21,‡] W. H. Toki,[21] R. J. Wilson,[21] D. D. Altenburg,[22] E. Feltresi,[22] A. Hauke,[22] H. Jasper,[22] M. Karbach,[22] J. Merkel,[22] A. Petzold,[22] B. Spaan,[22] K. Wacker,[22] M. J. Kobel,[23] W. F. Mader,[23] R. Nogowski,[23] K. R. Schubert,[23] R. Schwierz,[23] A. Volk,[23] D. Bernard,[24] G. R. Bonneaud,[24] E. Latour,[24] M. Verderi,[24] P. J. Clark,[25] S. Playfer,[25] J. E. Watson,[25] M. Andreotti,[26a,26b] D. Bettoni,[26a] C. Bozzi,[26a] R. Calabrese,[26a,26b] A. Cecchi,[26a,26b] G. Cibinetto,[26a,26b] P. Franchini,[26a,26b] E. Luppi,[26a,26b] M. Negrini,[26a,26b] A. Petrella,[26a,26b] L. Piemontese,[26a] V. Santoro,[26a,26b] R. Baldini-Ferroli,[27] A. Calcaterra,[27] R. de Sangro,[27] G. Finocchiaro,[27] S. Pacetti,[27] P. Patteri,[27] I. M. Peruzzi,[27,§] M. Piccolo,[27] M. Rama,[27] A. Zallo,[27] A. Buzzo,[28a] R. Contri,[28a,28b] M. Lo Vetere,[28a,28b] M. M. Macri,[28a] M. R. Monge,[28a,28b] S. Passaggio,[28a] C. Patrignani,[28a,28b] E. Robutti,[28a] A. Santroni,[28a,28b] S. Tosi,[28a,28b] K. S. Chaisanguanthum,[29] M. Morii,[29] A. Adametz,[30] J. Marks,[30] S. Schenk,[30] U. Uwer,[30] V. Klose,[31] H. M. Lacker,[31] D. J. Bard,[32] P. D. Dauncey,[32] J. A. Nash,[32] M. Tibbetts,[32] P. K. Behera,[33] X. Chai,[33] M. J. Charles,[33] U. Mallik,[33] J. Cochran,[34] H. B. Crawley,[34] L. Dong,[34] W. T. Meyer,[34] S. Prell,[34] E. I. Rosenberg,[34] A. E. Rubin,[34] Y. Y. Gao,[35] A. V. Gritsan,[35] Z. J. Guo,[35] C. K. Lae,[35] N. Arnaud,[36] J. Béquilleux,[36] A. D'Orazio,[36] M. Davier,[36] J. Firmino da Costa,[36] G. Grosdidier,[36] A. Höcker,[36] V. Lepeltier,[36] F. Le Diberder,[36] A. M. Lutz,[36] S. Pruvot,[36] P. Roudeau,[36] M. H. Schune,[36] J. Serrano,[36] V. Sordini,[36,‖] A. Stocchi,[36] G. Wormser,[36] D. J. Lange,[37] D. M. Wright,[37] I. Bingham,[38] J. P. Burke,[38] C. A. Chavez,[38] J. R. Fry,[38] E. Gabathuler,[38] R. Gamet,[38] D. E. Hutchcroft,[38] D. J. Payne,[38] C. Touramanis,[38] A. J. Bevan,[39] C. K. Clarke,[39] K. A. George,[39] F. Di Lodovico,[39] R. Sacco,[39] M. Sigamani,[39] G. Cowan,[40] H. U. Flaecher,[40] D. A. Hopkins,[40] S. Paramesvaran,[40] F. Salvatore,[40] A. C. Wren,[40] D. N. Brown,[41] C. L. Davis,[41] A. G. Denig,[42] M. Fritsch,[42] W. Gradl,[42] G. Schott,[42] K. E. Alwyn,[43] D. Bailey,[43] R. J. Barlow,[43] Y. M. Chia,[43] C. L. Edgar,[43] G. Jackson,[43] G. D. Lafferty,[43] T. J. West,[43] J. I. Yi,[43] J. Anderson,[44] C. Chen,[44] A. Jawahery,[44] D. A. Roberts,[44] G. Simi,[44] J. M. Tuggle,[44] C. Dallapiccola,[45] X. Li,[45] E. Salvati,[45] S. Saremi,[45] R. Cowan,[46] D. Dujmic,[46] P. H. Fisher,[46] G. Sciolla,[46] M. Spitznagel,[46] F. Taylor,[46] R. K. Yamamoto,[46] M. Zhao,[46] P. M. Patel,[47] S. H. Robertson,[47] A. Lazzaro,[48a,48b] V. Lombardo,[48a] F. Palombo,[48a,48b] J. M. Bauer,[49] L. Cremaldi,[49] R. Godang,[49,¶] R. Kroeger,[49] D. A. Sanders,[49] D. J. Summers,[49] H. W. Zhao,[49] M. Simard,[50] P. Taras,[50] F. B. Viaud,[50] H. Nicholson,[51] G. De Nardo,[52a,52b] L. Lista,[52a] D. Monorchio,[52a,52b] G. Onorato,[52a,52b] C. Sciacca,[52a,52b] G. Raven,[53] H. L. Snoek,[53] C. P. Jessop,[54] K. J. Knoepfel,[54] J. M. LoSecco,[54] W. F. Wang,[54] G. Benelli,[55] L. A. Corwin,[55] K. Honscheid,[55] H. Kagan,[55] R. Kass,[55] J. P. Morris,[55] A. M. Rahimi,[55] J. J. Regensburger,[55] S. J. Sekula,[55] Q. K. Wong,[55] N. L. Blount,[56] J. Brau,[56] R. Frey,[56] O. Igonkina,[56] J. A. Kolb,[56] M. Lu,[56] R. Rahmat,[56] N. B. Sinev,[56] D. Strom,[56] J. Strube,[56] E. Torrence,[56] G. Castelli,[57a,57b] N. Gagliardi,[57a,57b] M. Margoni,[57a,57b] M. Morandin,[57a] M. Posocco,[57a] M. Rotondo,[57a] F. Simonetto,[57a,57b] R. Stroili,[57a,57b] C. Voci,[57a,57b] P. del Amo Sanchez,[58] E. Ben-Haim,[58] H. Briand,[58] G. Calderini,[58] J. Chauveau,[58] P. David,[58] L. Del Buono,[58] O. Hamon,[58] Ph. Leruste,[58] J. Ocariz,[58] A. Perez,[58] J. Prendki,[58] S. Sitt,[58] L. Gladney,[59] M. Biasini,[60a,60b] R. Covarelli,[60a,60b] E. Manoni,[60a,60b] C. Angelini,[61a,61b] G. Batignani,[61a,61b] S. Bettarini,[61a,61b] M. Carpinelli,[61a,61b,**] A. Cervelli,[61a,61b] F. Forti,[61a,61b] M. A. Giorgi,[61a,61b] A. Lusiani,[61a,61c] G. Marchiori,[61a,61b] M. Morganti,[61a,61b] N. Neri,[61a,61b] E. Paoloni,[61a,61b] G. Rizzo,[61a,61b] J. J. Walsh,[61a] D. Lopes Pegna,[62] C. Lu,[62] J. Olsen,[62] A. J. S. Smith,[62] A. V. Telnov,[62] F. Anulli,[63a] E. Baracchini,[63a,63b] G. Cavoto,[63a] D. del Re,[63a,63b] E. Di Marco,[63a,63b] R. Faccini,[63a,63b] F. Ferrarotto,[63a] F. Ferroni,[63a,63b] M. Gaspero,[63a,63b] P. D. Jackson,[63a] L. Li Gioi,[63a] M. A. Mazzoni,[63a] S. Morganti,[63a]

G. Piredda,[63a] F. Polci,[63a,63b] F. Renga,[63a,63b] C. Voena,[63a] M. Ebert,[64] T. Hartmann,[64] H. Schröder,[64] R. Waldi,[64] T. Adye,[65] B. Franek,[65] E. O. Olaiya,[65] F. F. Wilson,[65] S. Emery,[66] M. Escalier,[66] L. Esteve,[66] S. F. Ganzhur,[66] G. Hamel de Monchenault,[66] W. Kozanecki,[66] G. Vasseur,[66] Ch. Yèche,[66] M. Zito,[66] X. R. Chen,[67] H. Liu,[67] W. Park,[67] M. V. Purohit,[67] R. M. White,[67] J. R. Wilson,[67] M. T. Allen,[68] D. Aston,[68] R. Bartoldus,[68] P. Bechtle,[68] J. F. Benitez,[68] R. Cenci,[68] J. P. Coleman,[68] M. R. Convery,[68] J. C. Dingfelder,[68] J. Dorfan,[68] G. P. Dubois-Felsmann,[68] W. Dunwoodie,[68] R. C. Field,[68] A. M. Gabareen,[68] S. J. Gowdy,[68] M. T. Graham,[68] P. Grenier,[68] C. Hast,[68] W. R. Innes,[68] J. Kaminski,[68] M. H. Kelsey,[68] H. Kim,[68] P. Kim,[68] M. L. Kocian,[68] D. W. G. S. Leith,[68] S. Li,[68] B. Lindquist,[68] S. Luitz,[68] V. Luth,[68] H. L. Lynch,[68] D. B. MacFarlane,[68] H. Marsiske,[68] R. Messner,[68] D. R. Muller,[68] H. Neal,[68] S. Nelson,[68] C. P. O'Grady,[68] I. Ofte,[68] A. Perazzo,[68] M. Perl,[68] B. N. Ratcliff,[68] A. Roodman,[68] A. A. Salnikov,[68] R. H. Schindler,[68] J. Schwiening,[68] A. Snyder,[68] D. Su,[68] M. K. Sullivan,[68] K. Suzuki,[68] S. K. Swain,[68] J. M. Thompson,[68] J. Va'vra,[68] A. P. Wagner,[68] M. Weaver,[68] C. A. West,[68] W. J. Wisniewski,[68] M. Wittgen,[68] D. H. Wright,[68] H. W. Wulsin,[68] A. K. Yarritu,[68] K. Yi,[68] C. C. Young,[68] V. Ziegler,[68] P. R. Burchat,[69] A. J. Edwards,[69] S. A. Majewski,[69] T. S. Miyashita,[69] B. A. Petersen,[69] L. Wilden,[69] S. Ahmed,[70] M. S. Alam,[70] J. A. Ernst,[70] B. Pan,[70] M. A. Saeed,[70] S. B. Zain,[70] S. M. Spanier,[71] B. J. Wogsland,[71] R. Eckmann,[72] J. L. Ritchie,[72] A. M. Ruland,[72] C. J. Schilling,[72] R. F. Schwitters,[72] B. W. Drummond,[73] J. M. Izen,[73] X. C. Lou,[73] F. Bianchi,[74a,74b] D. Gamba,[74a,74b] M. Pelliccioni,[74a,74b] M. Bomben,[75a,75b] L. Bosisio,[75a,75b] C. Cartaro,[75a,75b] G. Della Ricca,[75a,75b] L. Lanceri,[75a,75b] L. Vitale,[75a,75b] V. Azzolini,[76] N. Lopez-March,[76] F. Martinez-Vidal,[76] D. A. Milanes,[76] A. Oyanguren,[76] J. Albert,[77] Sw. Banerjee,[77] B. Bhuyan,[77] H. H. F. Choi,[77] K. Hamano,[77] R. Kowalewski,[77] M. J. Lewczuk,[77] I. M. Nugent,[77] J. M. Roney,[77] R. J. Sobie,[77] T. J. Gershon,[78] P. F. Harrison,[78] J. Ilic,[78] T. E. Latham,[78] G. B. Mohanty,[78] H. R. Band,[79] X. Chen,[79] S. Dasu,[79] K. T. Flood,[79] Y. Pan,[79] M. Pierini,[79] R. Prepost,[79] C. O. Vuosalo,[79] and S. L. Wu[79]

(*BABAR* Collaboration)

[1]*Laboratoire de Physique des Particules, IN2P3/CNRS et Université de Savoie, F-74941 Annecy-Le-Vieux, France*
[2]*Universitat de Barcelona, Facultat de Fisica, Departament ECM, E-08028 Barcelona, Spain*
[3a]*INFN Sezione di Bari, I-70126 Bari, Italy*
[3b]*Dipartmento di Fisica, Università di Bari, I-70126 Bari, Italy*
[4]*University of Bergen, Institute of Physics, N-5007 Bergen, Norway*
[5]*Lawrence Berkeley National Laboratory and University of California, Berkeley, California 94720, USA*
[6]*University of Birmingham, Birmingham, B15 2TT, United Kingdom*
[7]*Ruhr Universität Bochum, Institut für Experimentalphysik 1, D-44780 Bochum, Germany*
[8]*University of Bristol, Bristol BS8 1TL, United Kingdom*
[9]*University of British Columbia, Vancouver, British Columbia, Canada V6T 1Z1*
[10]*Brunel University, Uxbridge, Middlesex UB8 3PH, United Kingdom*
[11]*Budker Institute of Nuclear Physics, Novosibirsk 630090, Russia*
[12]*University of California at Irvine, Irvine, California 92697, USA*
[13]*University of California at Los Angeles, Los Angeles, California 90024, USA*
[14]*University of California at Riverside, Riverside, California 92521, USA*
[15]*University of California at San Diego, La Jolla, California 92093, USA*
[16]*University of California at Santa Barbara, Santa Barbara, California 93106, USA*
[17]*University of California at Santa Cruz, Institute for Particle Physics, Santa Cruz, California 95064, USA*
[18]*California Institute of Technology, Pasadena, California 91125, USA*
[19]*University of Cincinnati, Cincinnati, Ohio 45221, USA*
[20]*University of Colorado, Boulder, Colorado 80309, USA*
[21]*Colorado State University, Fort Collins, Colorado 80523, USA*
[22]*Technische Universität Dortmund, Fakultät Physik, D-44221 Dortmund, Germany*
[23]*Technische Universität Dresden, Institut für Kern- und Teilchenphysik, D-01062 Dresden, Germany*
[24]*Laboratoire Leprince-Ringuet, CNRS/IN2P3, Ecole Polytechnique, F-91128 Palaiseau, France*
[25]*University of Edinburgh, Edinburgh EH9 3JZ, United Kingdom*
[26a]*INFN Sezione di Ferrara, I-44100 Ferrara, Italy*
[26b]*Dipartimento di Fisica, Università di Ferrara, I-44100 Ferrara, Italy*
[27]*INFN Laboratori Nazionali di Frascati, I-00044 Frascati, Italy*
[28a]*INFN Sezione di Genova, I-16146 Genova, Italy*
[28b]*Dipartimento di Fisica, Università di Genova, I-16146 Genova, Italy*
[29]*Harvard University, Cambridge, Massachusetts 02138, USA*
[30]*Universität Heidelberg, Physikalisches Institut, Philosophenweg 12, D-69120 Heidelberg, Germany*

[31]*Humboldt-Universität zu Berlin, Institut für Physik, Newtonstr. 15, D-12489 Berlin, Germany*
[32]*Imperial College London, London, SW7 2AZ, United Kingdom*
[33]*University of Iowa, Iowa City, Iowa 52242, USA*
[34]*Iowa State University, Ames, Iowa 50011-3160, USA*
[35]*Johns Hopkins University, Baltimore, Maryland 21218, USA*
[36]*Laboratoire de l'Accélérateur Linéaire, IN2P3/CNRS et Université Paris-Sud 11, Centre Scientifique d'Orsay, B. P. 34, F-91898 Orsay Cedex, France*
[37]*Lawrence Livermore National Laboratory, Livermore, California 94550, USA*
[38]*University of Liverpool, Liverpool L69 7ZE, United Kingdom*
[39]*Queen Mary, University of London, London, E1 4NS, United Kingdom*
[40]*University of London, Royal Holloway and Bedford New College, Egham, Surrey TW20 0EX, United Kingdom*
[41]*University of Louisville, Louisville, Kentucky 40292, USA*
[42]*Johannes Gutenberg-Universität Mainz, Institut für Kernphysik, D-55099 Mainz, Germany*
[43]*University of Manchester, Manchester M13 9PL, United Kingdom*
[44]*University of Maryland, College Park, Maryland 20742, USA*
[45]*University of Massachusetts, Amherst, Massachusetts 01003, USA*
[46]*Massachusetts Institute of Technology, Laboratory for Nuclear Science, Cambridge, Massachusetts 02139, USA*
[47]*McGill University, Montréal, Québec, Canada H3A 2T8*
[48a]*INFN Sezione di Milano, I-20133 Milano, Italy*
[48b]*Dipartimento di Fisica, Università di Milano, I-20133 Milano, Italy*
[49]*University of Mississippi, University, Mississippi 38677, USA*
[50]*Université de Montréal, Physique des Particules, Montréal, Québec, Canada H3C 3J7*
[51]*Mount Holyoke College, South Hadley, Massachusetts 01075, USA*
[52a]*INFN Sezione di Napoli, I-80126 Napoli, Italy*
[52b]*Dipartimento di Scienze Fisiche, Università di Napoli Federico II, I-80126 Napoli, Italy*
[53]*NIKHEF, National Institute for Nuclear Physics and High Energy Physics, NL-1009 DB Amsterdam, The Netherlands*
[54]*University of Notre Dame, Notre Dame, Indiana 46556, USA*
[55]*Ohio State University, Columbus, Ohio 43210, USA*
[56]*University of Oregon, Eugene, Oregon 97403, USA*
[57a]*INFN Sezione di Padova, I-35131 Padova, Italy*
[57b]*Dipartimento di Fisica, Università di Padova, I-35131 Padova, Italy*
[58]*Laboratoire de Physique Nucléaire et de Hautes Energies, IN2P3/CNRS, Université Pierre et Marie Curie-Paris6, Université Denis Diderot-Paris7, F-75252 Paris, France*
[59]*University of Pennsylvania, Philadelphia, Pennsylvania 19104, USA*
[60a]*INFN Sezione di Perugia, I-06100 Perugia, Italy*
[60b]*Dipartimento di Fisica, Università di Perugia, I-06100 Perugia, Italy*
[61a]*INFN Sezione di Pisa, I-56127 Pisa, Italy*
[61b]*Dipartimento di Fisica, Università di Pisa, I-56127 Pisa, Italy*
[61c]*Scuola Normale Superiore di Pisa, I-56127 Pisa, Italy*
[62]*Princeton University, Princeton, New Jersey 08544, USA*
[63a]*INFN Sezione di Roma, I-00185 Roma, Italy*
[63b]*Dipartimento di Fisica, Università di Roma La Sapienza, I-00185 Roma, Italy*
[64]*Universität Rostock, D-18051 Rostock, Germany*
[65]*Rutherford Appleton Laboratory, Chilton, Didcot, Oxon, OX11 0QX, United Kingdom*
[66]*CEA, Irfu, SPP, Centre de Saclay, F-91191 Gif-sur-Yvette, France*
[67]*University of South Carolina, Columbia, South Carolina 29208, USA*
[68]*Stanford Linear Accelerator Center, Stanford, California 94309, USA*
[69]*Stanford University, Stanford, California 94305-4060, USA*
[70]*State University of New York, Albany, New York 12222, USA*
[71]*University of Tennessee, Knoxville, Tennessee 37996, USA*
[72]*University of Texas at Austin, Austin, Texas 78712, USA*
[73]*University of Texas at Dallas, Richardson, Texas 75083, USA*

[*]Deceased.
[†]Present address: Temple University, Philadelphia, PA 19122, USA.
[‡]Present address: Tel Aviv University, Tel Aviv, 69978, Israel.
[§]Also at Università di Perugia, Dipartimento di Fisica, Perugia, Italy.
[‖]Also at Università di Roma La Sapienza, I-00185 Roma, Italy.
[¶]Present address: University of South Alabama, Mobile, AL 36688, USA.
[**]Also at Università di Sassari, Sassari, Italy.

[74a]*INFN Sezione di Torino, I-10125 Torino, Italy*
[74b]*Dipartimento di Fisica Sperimentale, Università di Torino, I-10125 Torino, Italy*
[75a]*INFN Sezione di Trieste, I-34127 Trieste, Italy*
[75b]*Dipartimento di Fisica, Università di Trieste, I-34127 Trieste, Italy*
[76]*IFIC, Universitat de Valencia-CSIC, E-46071 Valencia, Spain*
[77]*University of Victoria, Victoria, British Columbia, Canada V8W 3P6*
[78]*Department of Physics, University of Warwick, Coventry CV4 7AL, United Kingdom*
[79]*University of Wisconsin, Madison, Wisconsin 53706, USA*
(Received 26 August 2008; published 18 November 2008)

We perform a time-dependent and time-integrated angular analysis of the decays $B^0 \to \varphi K^*(892)^0$, $\varphi K_2^*(1430)^0$, and $\varphi(K\pi)_0^{*0}$ with the final sample of about 465×10^6 $B\bar{B}$ pairs recorded with the *BABAR* detector. Twenty-four parameters are investigated, including the branching fractions, *CP*-violation parameters, and parameters sensitive to final-state interactions. We use the dependence on the $K\pi$ invariant mass of the interference between the scalar and vector or tensor components to resolve discrete ambiguities of the strong and weak phases. We use the time evolution of the $B \to \varphi K_S^0 \pi^0$ channel to extract the *CP*-violation phase difference $\Delta\phi_{00} = 0.28 \pm 0.42 \pm 0.04$ between the B and $\bar{B}$ decay amplitudes. When the $B \to \varphi K^\pm \pi^\mp$ channel is included, the fractions of longitudinal polarization f_L of the vector-vector and vector-tensor decay modes are measured to be $0.494 \pm 0.034 \pm 0.013$ and $0.901^{+0.046}_{-0.058} \pm 0.037$, respectively. This polarization pattern requires the presence of a positive-helicity amplitude in the vector-vector decay from a currently unknown source.

DOI: 10.1103/PhysRevD.78.092008 PACS numbers: 13.25.Hw, 11.30.Er, 12.15.Hh, 13.88.+e

I. INTRODUCTION

Charge-parity (*CP*) symmetry violation has been recognized as one of the fundamental requirements for producing a matter-dominated universe [1] and therefore it has played an important role in understanding fundamental physics since its initial discovery in the K meson system in 1964 [2]. A significant *CP*-violating asymmetry has been observed in decays of neutral B mesons to final states containing charmonium, due to interference between B^0-$\bar{B}^0$ mixing and direct decay amplitudes [3]. It has been established [4] that the *CP*-violating decays of the K_L^0 meson are due to *CP* violation in decay amplitudes, as well as in K^0-$\bar{K}^0$ mixing, and this kind of "direct" *CP* asymmetry in B decays has also been observed recently [5]. The *CP* asymmetries are generally much larger in B decays than in K decays [6] because they directly probe the least flat unitarity triangle constructed from the Cabibbo-Kobayashi-Maskawa (CKM) matrix elements V_{ij}, which relate weak and flavor quark eigenstates [7]. This triangle reflects the unitarity of the CKM matrix, and two of its angles are the phase differences of its sides on the complex plane: $\alpha \equiv \arg(-V_{td}V_{tb}^*/V_{ud}V_{ub}^*)$ and $\beta \equiv \arg(-V_{cd}V_{cb}^*/V_{td}V_{tb}^*)$. Because of the large *CP*-violating effects, B decays provide an excellent testing ground of fundamental interactions.

The *CP*-violating effects observed to date are self-consistent within the standard model with a single complex phase in the CKM mechanism [7]. However, this mechanism alone is believed to be insufficient to produce the present matter-dominated Universe. Therefore, it is important to search for new sources of *CP*-violating interactions. While direct access to new fundamental particles and interactions may be beyond the energy reach of operating accelerators, one can look for them in virtual transitions. New particles in virtual transitions, including but not limited to supersymmetric particles [8], would provide additional amplitudes with different phases. Depending on the model parameters, sizable *CP*-violating effects, either B^0-$\bar{B}^0$ mixing-induced or direct, could be observed in pure penguin modes which involve virtual loops as in the example shown in Fig. 1. Some of the first observed gluonic penguin decays, $\overset{(-)}{B} \to \eta' \overset{(-)}{K}$ [9] and $\overset{(-)}{B} \to \varphi \overset{(-)}{K}{}^{(*)}$ [10], remain promising channels in which to look for new physics. The latter type of decay is illustrated in Fig. 1 and is the focus of this paper. For example, comparison of the value of $\sin 2\beta$ obtained from these modes with that from charmonium modes such as $\overset{(-)}{B} \to J/\psi \overset{(-)}{K}{}^{(*)}$ [3,11], or measurement of direct *CP* violation, can probe new physics participating in penguin loops [12].

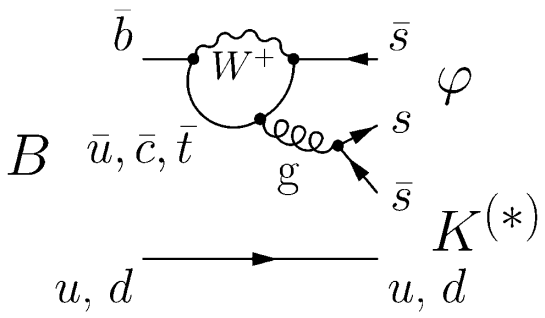

FIG. 1. Penguin diagram describing the decay $B \to \varphi K^{(*)}$.

The $(V\text{-}A)$ nature of the weak interaction leads to left-handed fermion couplings in interactions with W bosons, such as those shown in Fig. 1. Combined with helicity conservation in strong interactions and spin-flip suppression of relativistic decay products, this leads to certain expectations of the spin alignment in weak B meson decays to light particles with spin, such as $\overset{(-)}{B} \to \varphi \overset{(-)}{K}{}^*$ [13]. However, the large fraction of transverse polarization in the $\overset{(-)}{B} \to \varphi \overset{(-)}{K}{}^*(892)$ decay measured by *BABAR* [14] and by Belle [15] indicates a significant departure from the naive expectation of predominant longitudinal polarization. This suggests the presence of other contributions to the decay amplitude, previously neglected, either within or beyond the standard model [16]. The presence of a substantial transverse amplitude also allows the study of CP violation in the angular distribution of $\overset{(-)}{B} \to \varphi \overset{(-)}{K}{}^*$ decays, an approach complementary to either mixing-induced or yield asymmetry studies. Polarization measurements in B decays are discussed in a recent review [17,18]. In Table I, we list *BABAR*'s recent measurements of the branching fraction and longitudinal polarization in the decays $\overset{(-)}{B} \to \varphi \overset{(-)}{K}{}^{(*)}_J$ [19–23]. Measurements in $\overset{(-)}{B} \to \rho \overset{(-)}{K}{}^*$ decays have also revealed a large fraction of transverse polarization [24].

In this analysis, we use the final sample of about 465×10^6 $\Upsilon(4S) \to B\bar{B}$ pairs recorded with the *BABAR* detector at the PEP-II asymmetric-energy e^+e^- storage rings at Stanford Linear Accelerator Center (SLAC). We employ all of these techniques for CP-violation and polarization measurements in the study of a single B-decay topology $\overset{(-)}{B}{}^0 \to \varphi(\overset{(-)}{K}\pi)$. Overall, 27 independent parameters sensitive to CP violation, spin alignment, or strong- or weak-interaction phases describe three decay channels (twelve in either vector-vector or vector-tensor and three in vector-scalar decays), which leaves only one overall phase unmeasurable. The three channels in our amplitude analysis are $\overset{(-)}{B}{}^0 \to \varphi \overset{(-)}{K}{}^*(892)^0$, $\varphi \overset{(-)}{K}{}^*_2(1430)^0$, and $\varphi(\overset{(-)}{K}\pi)^{*0}_0$. The latter contribution includes the $\overset{(-)}{K}{}^*_0(1430)^0$ resonance together with a nonresonant component, as measured by the LASS experiment [25]. While we describe the analysis of these three neutral-B meson decays, this technique, with the exception of time-dependent measurements, has also been applied recently to the charged-B meson decays [21,22].

We use the time evolution of the $\overset{(-)}{B}{}^0 \to \varphi K^0_S \pi^0$ channel to extract the mixing-induced CP-violating phase difference between the B and $\bar{B}$ decay amplitudes, which is equivalent to a measurement of $\sin 2\beta$ to a good approximation. With the $\overset{(-)}{B}{}^0 \to \varphi K^{\pm}\pi^{\mp}$ channel included, the fractions of longitudinal and parity-odd transverse amplitudes in the vector-vector and vector-tensor decay modes are measured. We use the dependence on the $K\pi$ invariant mass of the interference between the scalar and vector or scalar and tensor components to resolve discrete ambiguities of the strong and weak phases. Using either interference between different channels or B^0-$\bar{B}^0$ mixing, we measure essentially all 27 independent parameters except for three quantities that characterize the parity-odd transverse amplitude in the vector-tensor decay, which is found to be consistent with zero.

TABLE I. *BABAR*'s recent measurements of the branching fraction $\mathcal{B}$ and longitudinal polarization fraction f_L in the decays $B \to \varphi K^{(*)}_J$. The spin J and parity P quantum numbers of the $K^{(*)}_J$ mesons are quoted. The upper limits are shown at the 90% confidence level. For a complete list of all observables in each analysis see the references listed. Results indicated with † are superseded by this analysis.

Mode	J^P	Ref.	$\mathcal{B}(10^{-6})$	f_L
φK^0	0^-	[19]	$8.4^{+1.5}_{-1.3} \pm 0.5$	1
φK^+	0^-	[19]	$10.0^{+0.9}_{-0.8} \pm 0.5$	1
$\varphi K^*_0(1430)^0$	0^+	[20]†	$4.6 \pm 0.7 \pm 0.6$	1
$\varphi K^*_0(1430)^+$	0^+	[21]	$7.0 \pm 1.3 \pm 0.9$	1
$\varphi K^*(892)^0$	1^-	[20]†	$9.2 \pm 0.7 \pm 0.6$	$0.51 \pm 0.04 \pm 0.02$
$\varphi K^*(892)^+$	1^-	[22]	$11.2 \pm 1.0 \pm 0.9$	$0.49 \pm 0.05 \pm 0.03$
$\varphi K^*(1410)^+$	1^-	[21]	<4.3	
$\varphi K^*(1680)^0$	1^-	[23]	<3.5	
$\varphi K_1(1270)^+$	1^+	[21]	$6.1 \pm 1.6 \pm 1.1$	$0.46^{+0.12+0.06}_{-0.13-0.07}$
$\varphi K_1(1400)^+$	1^+	[21]	<3.2	
$\varphi K^*_2(1430)^0$	2^+	[20]†	$7.8 \pm 1.1 \pm 0.6$	$0.85^{+0.06}_{-0.07} \pm 0.04$
$\varphi K^*_2(1430)^+$	2^+	[21]	$8.4 \pm 1.8 \pm 1.0$	$0.80^{+0.09}_{-0.10} \pm 0.03$
$\varphi K_2(1770)^+$	2^-	[21]	<15.0	
$\varphi K_2(1820)^+$	2^-	[21]	<16.3	
$\varphi K^*_3(1780)^0$	3^-	[23]	<2.7	
$\varphi K^*_4(2045)^0$	4^+	[23]	<15.3	

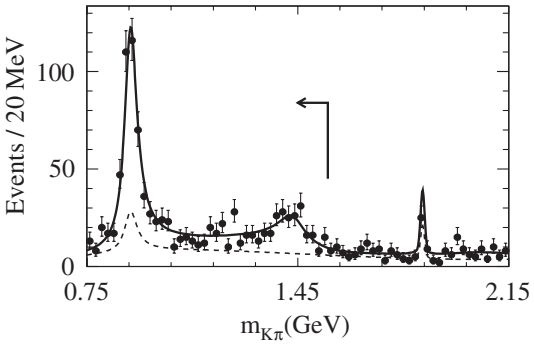

FIG. 2. Invariant $K\pi$ mass distribution from the $B \to \varphi K^{\pm}\pi^{\mp}$ analysis from Refs. [20,23]. The solid (dashed) line is a projection of the signal-plus-background (background only) fit result. The narrow charm background peak at 1.865 GeV comes from $\bar{D}^0$ decays to $K\pi$ and is not associated with $\varphi K^{\pm}\pi^{\mp}$ production. The arrow indicates the mass range considered in this analysis.

II. ANALYSIS STRATEGY

Earlier studies of $\overset{(-)}{B}{}^0 \to \varphi K^{\pm}\pi^{\mp}$ decays by the *BABAR* Collaboration [20,23] indicate the presence of three significant $K\pi$ partial waves: $(K\pi)^{*0}_0$ [spin $J = 0$, including the resonance $K^*_0(1430)^0$], $K^*(892)^0$ $(J = 1)$, and $K^*_2(1430)^0$ $(J = 2)$. These correspond to the following decays, with the number of independent amplitudes characterizing different spin projections given in parentheses: $\overset{(-)}{B}{}^0 \to \varphi(\overset{(-)}{K}\pi)^{*0}_0$ (one), $\varphi\overset{(-)}{K}{}^*(892)^0$ (three), and $\varphi\overset{(-)}{K}{}^*_2(1430)^0$ (three). No significant contribution from other final states has been found with $K\pi$ invariant mass $m_{K\pi}$ up to 2.15 GeV [21,23]. See Fig. 2 for an illustration of the $\overset{(-)}{B}{}^0 \to \varphi K^{\pm}\pi^{\mp}$ contributions. Therefore, we limit our analysis to the mass range $m_{K\pi} < 1.55$ GeV without any significant loss of $\overset{(-)}{B}{}^0 \to \varphi K^{\pm}\pi^{\mp}$ signal through charmless $K\pi$ resonant or nonresonant production.

There has been no extensive study of the $\overset{(-)}{B}{}^0 \to \varphi K^0_S\pi^0$ decay, except for the study of $\overset{(-)}{B}{}^0 \to \varphi\overset{(-)}{K}{}^*(892)^0$ [14]. However, due to isospin symmetry of the $K^0\pi^0$ and $K^{\pm}\pi^{\mp}$ systems, the same amplitude composition is expected in the $\varphi K^{\pm}\pi^{\mp}$ and $\varphi K^0_S\pi^0$ final states. We do not expect any charmless resonance structure in the $\varphi K^{\pm}$ or $\varphi\pi^{\mp}$ combinations, while we veto the charm resonance states, such as $D^{\pm}_{(s)} \to \varphi\pi^{\pm}$.

It is instructive to do a simple counting of the amplitude parameters in $\overset{(-)}{B}{}^0 \to \varphi\overset{(-)}{K}\pi$ decays with the three $K\pi$ spin contributions discussed above. With seven independent $A_{J\lambda}$ complex amplitudes for B decays and seven $\bar{A}_{J\lambda}$ amplitudes for $\bar{B}$ decays, we could construct 28 independent real parameters. Here J refers to the spin of the $K\pi$ system and λ to the spin projection of the φ meson onto the direction opposite to the B meson flight direction in the φ rest frame. However, one overall phase is not measurable and we are left with 27 real measurable parameters. Among these parameters, 26 parameters have been or can be measured in the decay $\overset{(-)}{B}{}^0 \to \varphi K^{\pm}\pi^{\mp}$ [20]. Those are branching fractions, polarization parameters, strong phases, and CP asymmetries. Some of the phases are extracted from the interference effects between different modes. However, due to limited statistics some of the CP asymmetries were not measured in earlier analyses and we now extend those measurements.

TABLE II. Definitions of 27 real parameters measurable with the $B^0 \to \varphi K\pi$ decays. Three resonance final states with spin $J = 0, 1, 2$ are considered in the $K\pi$ spectrum. The branching fraction $\mathcal{B}$ is calculated as a ratio of the average partial decay widths for $B^0(\Gamma)$ and $\bar{B}^0(\bar{\Gamma})$ and the total width $\Gamma_{\rm total}$ where we neglect any difference in the B^0 and $\bar{B}^0$ widths. This definition allows for differences between the B^0 and $\bar{B}^0$ decay amplitudes, $A_{J\lambda}$ and $\bar{A}_{J\lambda}$, as discussed in the text.

Parameter	Definition	$\varphi K^*_0(1430)$ $J = 0$	$\varphi K^*(892)$ $J = 1$	$\varphi K^*_2(1430)$ $J = 2$
$\mathcal{B}_J$	$\frac{1}{2}(\bar{\Gamma}_J + \Gamma_J)/\Gamma_{\rm total}$	$\mathcal{B}_0$	$\mathcal{B}_1$	$\mathcal{B}_2$
f_{LJ}	$\frac{1}{2}(\lvert\bar{A}_{J0}\rvert^2/\Sigma\lvert\bar{A}_{J\lambda}\rvert^2 + \lvert A_{J0}\rvert^2/\Sigma\lvert A_{J\lambda}\rvert^2)$	1	f_{L1}	f_{L2}
$f_{\perp J}$	$\frac{1}{2}(\lvert\bar{A}_{J\perp}\rvert^2/\Sigma\lvert\bar{A}_{J\lambda}\rvert^2 + \lvert A_{J\perp}\rvert^2/\Sigma\lvert A_{J\lambda}\rvert^2)$	None	$f_{\perp 1}$	$f_{\perp 2}$
$\phi_{\parallel J}$	$\frac{1}{2}(\arg(\bar{A}_{J\parallel}/\bar{A}_{J0}) + \arg(A_{J\parallel}/A_{J0}))$	None	$\phi_{\parallel 1}$	$\phi_{\parallel 2}$
$\phi_{\perp J}$	$\frac{1}{2}(\arg(\bar{A}_{J\perp}/\bar{A}_{J0}) + \arg(A_{J\perp}/A_{J0}) - \pi)$	None	$\phi_{\perp 1}$	$\phi_{\perp 2}$
δ_{0J}	$\frac{1}{2}(\arg(\bar{A}_{00}/\bar{A}_{J0}) + \arg(A_{00}/A_{J0}))$	0	δ_{01}	δ_{02}
$\mathcal{A}_{CPJ}$	$(\bar{\Gamma}_J - \Gamma_J)/(\bar{\Gamma}_J + \Gamma_J)$	$\mathcal{A}_{CP0}$	$\mathcal{A}_{CP1}$	$\mathcal{A}_{CP2}$
$\mathcal{A}^0_{CPJ}$	$(\lvert\bar{A}_{J0}\rvert^2/\Sigma\lvert\bar{A}_{J\lambda}\rvert^2 - \lvert A_{J0}\rvert^2/\Sigma\lvert A_{J\lambda}\rvert^2)/(\lvert\bar{A}_{J0}\rvert^2/\Sigma\lvert\bar{A}_{J\lambda}\rvert^2 + \lvert A_{J0}\rvert^2/\Sigma\lvert A_{J\lambda}\rvert^2)$	0	$\mathcal{A}^0_{CP1}$	$\mathcal{A}^0_{CP2}$
$\mathcal{A}^{\perp}_{CPJ}$	$(\lvert\bar{A}_{J\perp}\rvert^2/\Sigma\lvert\bar{A}_{J\lambda}\rvert^2 - \lvert A_{J\perp}\rvert^2/\Sigma\lvert A_{J\lambda}\rvert^2)/(\lvert\bar{A}_{J\perp}\rvert^2/\Sigma\lvert\bar{A}_{J\lambda}\rvert^2 + \lvert A_{J\perp}\rvert^2/\Sigma\lvert A_{J\lambda}\rvert^2)$	None	$\mathcal{A}^{\perp}_{CP1}$	$\mathcal{A}^{\perp}_{CP2}$
$\Delta\phi_{\parallel J}$	$\frac{1}{2}(\arg(\bar{A}_{J\parallel}/\bar{A}_{J0}) - \arg(A_{J\parallel}/A_{J0}))$	None	$\Delta\phi_{\parallel 1}$	$\Delta\phi_{\parallel 2}$
$\Delta\phi_{\perp J}$	$\frac{1}{2}(\arg(\bar{A}_{J\perp}/\bar{A}_{J0}) - \arg(A_{J\perp}/A_{J0}) - \pi)$	None	$\Delta\phi_{\perp 1}$	$\Delta\phi_{\perp 2}$
$\Delta\delta_{0J}$	$\frac{1}{2}(\arg(\bar{A}_{00}/\bar{A}_{J0}) - \arg(A_{00}/A_{J0}))$	0	$\Delta\delta_{01}$	$\Delta\delta_{02}$
$\Delta\phi_{00}$	$\frac{1}{2}\arg(A_{00}/\bar{A}_{00})$	$\Delta\phi_{00}$	None	None

Finally, one parameter, which relates the phases of the B and $\bar{B}$ decay amplitudes, can be measured using only the interference between decays with and without B^0-$\bar{B}^0$ mixing, to final states which can be decomposed as CP eigenstates, such as $\varphi K^0_S \pi^0$. In Table II all 27 real parameters measurable with $\overset{(-)}{B}{}^0 \to \varphi \overset{(-)}{K} \pi$ decays are summarized. These parameters are expressed in terms of the $A_{J\lambda}$ and $\bar{A}_{J\lambda}$ amplitudes for $B^0 \to \varphi K^+ \pi^-$ or $\varphi K^0 \pi^0$ and $\bar{B}^0 \to \varphi K^- \pi^+$ or $\varphi \bar{K}^0 \pi^0$ decays. We also refer to a transformed set of amplitudes A_{J0} and $A_{J\pm 1} = (A_{J\parallel} \pm A_{J\perp})/\sqrt{2}$. The parameters in Table II are expressed as six CP-averaged and six CP-violating parameters for the vector-vector and vector-tensor decays. The π in the definitions of $\phi_{\perp J}$ and $\Delta\phi_{\perp J}$ accounts for the sign flip $A_{\perp J} = -\bar{A}_{\perp J}$ if CP is conserved. The parametrization in Table II is motivated by the negligible CP violation expected in these decays. Therefore, the polarization parameters specific to either B (superscript "$-$") or $\bar{B}$ (superscript "$+$") are the CP-averaged parameters with small CP-violating corrections which are either multiplicative (for rates) or additive (for phases):

$$\mathcal{B}^{\pm}_J = \mathcal{B}_J \cdot (1 \pm \mathcal{A}_{CPJ})/2, \tag{1}$$

$$f^{\pm}_{LJ} = f_{LJ} \cdot (1 \pm \mathcal{A}^0_{CPJ}), \tag{2}$$

$$f^{\pm}_{\perp J} = f_{\perp J} \cdot (1 \pm \mathcal{A}^{\perp}_{CPJ}), \tag{3}$$

$$\phi^{\pm}_{\parallel J} = \phi_{\parallel J} \pm \Delta\phi_{\parallel J}, \tag{4}$$

$$\phi^{\pm}_{\perp J} = \phi_{\perp J} \pm \Delta\phi_{\perp J} + \frac{\pi}{2} \pm \frac{\pi}{2}, \tag{5}$$

$$\delta^{\pm}_{0J} = \delta_{0J} \pm \Delta\delta_{0J}. \tag{6}$$

In this section we discuss further the method for the measurement of the relative phase, along with all of the other parameters. First we review the angular distributions, follow with a discussion of the $K\pi$ invariant mass distributions critical to separating different partial waves, then introduce interference effects between amplitudes from different decays, and finally discuss time-dependent distributions.

A. Angular distributions

We discuss here the angular distribution of the decay products in the chain $B \to \varphi K^* \to (K^+K^-)(K\pi)$ integrated over time. First we look at the decay of a B meson only and leave the $\bar{B}$ for later discussion, which involves CP violation. Angular momentum conservation in the decay of a spinless B meson leads to three possible spin projections of the φ meson onto its direction of flight, each corresponding to a complex amplitude $A_{J\lambda}$ with $\lambda = 0$ or ± 1. The three λ values are allowed with the K^* spin states $J \geq 1$, but only $\lambda = 0$ contributes with a spin-zero K^*. The angular distributions can be expressed as functions of $\mathcal{H}_i = \cos\theta_i$ and Φ. Here θ_i is the angle between the direction of the K meson from the $K^* \to K\pi$ (θ_1) or $\varphi \to K\bar{K}$ (θ_2) and the direction opposite to the B in the K^* or φ rest frame, and Φ is the angle between the decay planes of the two systems, as shown in Fig. 3. The differential decay width is

$$\frac{d^3\Gamma}{d\mathcal{H}_1 d\mathcal{H}_2 d\Phi} \propto \left| \sum A_{J\lambda} Y^{\lambda}_J(\mathcal{H}_1, \Phi) Y^{-\lambda}_1(-\mathcal{H}_2, 0) \right|^2, \tag{7}$$

where Y^{λ}_J are the spherical harmonic functions, with $J = 2$ for $K^*_2(1430)$, $J = 1$ for $K^*(892)$, and $J = 0$ for $(K\pi)^*_0$, including $K^*_0(1430)$. We do not consider higher values of J because no significant contribution from those states is expected. Only resonances with spin-parity combination $P = (-1)^J$ are possible in the decay $K^* \to K\pi$ due to parity conservation in these strong-interaction decays.

If we ignore interference between modes with different spins J of the $K\pi$ system in Eq. (7), then for each decay mode we have three complex amplitudes $A_{J\lambda}$ which appear in the angular distribution. We discuss interference between different modes later in this section. The differential decay rate for each decay mode involves six real quantities α^-_{iJ}, including terms that account for interference between amplitudes of common J:

$$\frac{d^3\Gamma_J}{\Gamma_J d\mathcal{H}_1 d\mathcal{H}_2 d\Phi} = \sum_i \alpha^-_{iJ} f_{iJ}(\mathcal{H}_1, \mathcal{H}_2, \Phi), \tag{8}$$

where the functions $f_{iJ}(\mathcal{H}_1, \mathcal{H}_2, \Phi)$ are given in Table III. The α^-_{iJ} parameters are defined as

$$\alpha^-_{1J} = \frac{|A_{J0}|^2}{\Sigma|A_{J\lambda}|^2} = f^-_{LJ}, \tag{9}$$

$$\alpha^-_{2J} = \frac{|A_{J\parallel}|^2 + |A_{J\perp}|^2}{\Sigma|A_{J\lambda}|^2} = \frac{|A_{J+1}|^2 + |A_{J-1}|^2}{\Sigma|A_{J\lambda}|^2} = (1 - f^-_{LJ}), \tag{10}$$

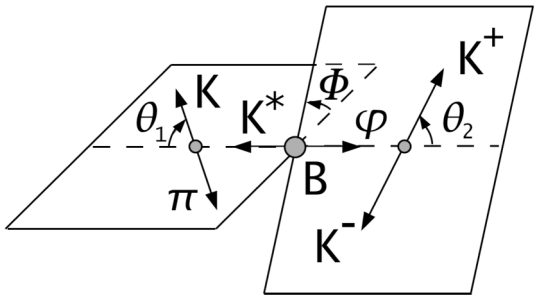

FIG. 3. Definition of decay angles given in the rest frames of the decaying parents.

TABLE III. Parametrization of the angular distribution in Eq. (8) in the $B^0 \to \varphi(K\pi)_J$ decays where three resonance final states with spin $J = 0, 1, 2$ are considered. The common constant is quoted for each decay mode and is omitted from each individual function below. The three helicity angle parameters ($\mathcal{H}_1, \mathcal{H}_2, \Phi$) are discussed in the text.

	$\varphi K_0^*(1430)^0$ $J=0$	$\varphi K^*(892)^0$ $J=1$	$\varphi K_2^*(1430)^0$ $J=2$
Common constant	$3/4\pi$	$9/8\pi$	$15/32\pi$
$f_{1J}(\mathcal{H}_1, \mathcal{H}_2, \Phi)$	$\mathcal{H}_2^2$	$\mathcal{H}_1^2\mathcal{H}_2^2$	$(3\mathcal{H}_1^2 - 1)^2\mathcal{H}_2^2$
$f_{2J}(\mathcal{H}_1, \mathcal{H}_2, \Phi)$	0	$\frac{1}{4}(1 - \mathcal{H}_1^2)(1 - \mathcal{H}_2^2)$	$3\mathcal{H}_1^2(1 - \mathcal{H}_1^2)(1 - \mathcal{H}_2^2)$
$f_{3J}(\mathcal{H}_1, \mathcal{H}_2, \Phi)$	0	$\frac{1}{4}(1 - \mathcal{H}_1^2)(1 - \mathcal{H}_2^2)\cos 2\Phi$	$3\mathcal{H}_1^2(1 - \mathcal{H}_1^2)(1 - \mathcal{H}_2^2)\cos 2\Phi$
$f_{4J}(\mathcal{H}_1, \mathcal{H}_2, \Phi)$	0	$-\frac{1}{2}(1 - \mathcal{H}_1^2)(1 - \mathcal{H}_2^2)\sin 2\Phi$	$-6\mathcal{H}_1^2(1 - \mathcal{H}_1^2)(1 - \mathcal{H}_2^2)\sin 2\Phi$
$f_{5J}(\mathcal{H}_1, \mathcal{H}_2, \Phi)$	0	$\sqrt{2}\mathcal{H}_1\sqrt{1 - \mathcal{H}_2^2}\mathcal{H}_2\sqrt{1 - \mathcal{H}_2^2}\cos\Phi$	$\sqrt{6}\mathcal{H}_1\sqrt{1 - \mathcal{H}_1^2}(3\mathcal{H}_1^2 - 1)\mathcal{H}_2\sqrt{1 - \mathcal{H}_2^2}\cos\Phi$
$f_{6J}(\mathcal{H}_1, \mathcal{H}_2, \Phi)$	0	$-\sqrt{2}\mathcal{H}_1\sqrt{1 - \mathcal{H}_1^2}\mathcal{H}_2\sqrt{1 - \mathcal{H}_2^2}\sin\Phi$	$-\sqrt{6}\mathcal{H}_1\sqrt{1 - \mathcal{H}_1^2}(3\mathcal{H}_1^2 - 1)\mathcal{H}_2\sqrt{1 - \mathcal{H}_2^2}\sin\Phi$

$$\alpha_{3J}^- = \frac{|A_{J\parallel}|^2 - |A_{J\perp}|^2}{\Sigma|A_{J\lambda}|^2} = 2 \cdot \frac{\Re e(A_{J+1}A_{J-1}^*)}{\Sigma|A_{J\lambda}|^2} = (1 - f_{LJ}^- - 2 \cdot f_{\perp J}^-), \quad (11)$$

$$\alpha_{4J}^- = \frac{\Im m(A_{J\perp}A_{J\parallel}^*)}{\Sigma|A_{J\lambda}|^2} = \frac{\Im m(A_{J+1}A_{J-1}^*)}{\Sigma|A_{J\lambda}|^2} = \sqrt{f_{\perp J}^- \cdot (1 - f_{LJ}^- - f_{\perp J}^-)} \cdot \sin(\phi_{\perp J}^- - \phi_{\parallel J}^-), \quad (12)$$

$$\alpha_{5J}^- = \frac{\Re e(A_{J\parallel}A_{J0}^*)}{\Sigma|A_{J\lambda}|^2} = \frac{\Re e(A_{J+1}A_{J0}^* + A_{J-1}A_{J0}^*)}{\sqrt{2} \cdot \Sigma|A_{J\lambda}|^2} = \sqrt{f_{LJ}^- \cdot (1 - f_{LJ}^- - f_{\perp J}^-)} \cdot \cos(\phi_{\parallel J}^-), \quad (13)$$

$$\alpha_{6J}^- = \frac{\Im m(A_{J\perp}A_{J0}^*)}{\Sigma|A_{J\lambda}|^2} = \frac{\Im m(A_{J+1}A_{J0}^* - A_{J-1}A_{J0}^*)}{\sqrt{2} \cdot \Sigma|A_{J\lambda}|^2} = \sqrt{f_{\perp J}^- \cdot f_{LJ}^-} \cdot \sin(\phi_{\perp J}^-). \quad (14)$$

The above terms are specific to the B^0 decays and are denoted with the superscript "$^-$," as introduced in Eqs. (1)–(6). The angular distributions for the $\bar{B}^0$ decays are described by the same Eq. (8), but with α_{iJ}^- replaced by α_{iJ}^+, and with definitions given by Eqs. (9)–(14), replacing A by $\bar{A}$ and superscript "$^-$" by "$^+$."

B. Mass distributions

The differential decay width given in Eq. (7) is parametrized as a function of helicity angles. However, it also depends on the invariant mass $m_{K\pi}$ of the $K\pi$ resonance, and the amplitudes should be considered as functions of $m_{K\pi}$. Without considering interference between different modes, as shown in Eq. (8), this mass dependence decouples from the angular dependence. Nonetheless, this dependence is important for separating different $K\pi$ states. The interference effects will be considered in the next subsection. A relativistic spin-J Breit-Wigner (B-W) complex amplitude R_J can be used to parametrize the resonance masses with $J = 1$ and $J = 2$ [18]:

$$R_J(m) = \frac{m_J\Gamma_J(m)}{(m_J^2 - m^2) - im_J\Gamma_J(m)} = \sin\delta_J e^{i\delta_J}, \quad (15)$$

where we use the following convention:

$$\cot\delta_J = \frac{m_J^2 - m^2}{m_J\Gamma_J(m)}. \quad (16)$$

The mass-dependent widths are given by

$$\Gamma_1(m) = \Gamma_1 \frac{m_1}{m} \frac{1 + r^2q_1^2}{1 + r^2q^2}\left(\frac{q}{q_1}\right)^3, \quad (17)$$

$$\Gamma_2(m) = \Gamma_2 \frac{m_2}{m} \frac{9 + 3r^2q_2^2 + r^4q_2^4}{3 + 3r^2q^2 + r^4q^4}\left(\frac{q}{q_2}\right)^5, \quad (18)$$

where Γ_J is the resonance width, m_J is the resonance mass, q is the momentum of a daughter particle in the resonance system after its two-body decay (q_J is evaluated at $m = m_J$), and r is the interaction radius.

The parametrization of the scalar $(K\pi)_0^{*0}$ mass distribution requires more attention. Studies of $K\pi$ scattering were performed by the LASS experiment [25]. It was found that the scattering is elastic up to about 1.5 GeV and can be parametrized with the amplitude:

$$R_0(m) = \sin\delta_0 e^{i\delta_0}, \quad (19)$$

where

$$\delta_0 = \Delta R + \Delta B, \quad (20)$$

ΔR represents a resonant $K_0^*(1430)^0$ contribution and ΔB represents a nonresonant contribution. The mass dependence of ΔB is described by means of an effective range parametrization of the usual type:

$$\cot\Delta B = \frac{1}{aq} + \frac{1}{2}bq, \quad (21)$$

where a is the scattering length and b is the effective range. The mass dependence of ΔR is described by means of a

B-W parametrization of a form similar to Eq. (16):

$$\cot\Delta R = \frac{m_0^2 - m^2}{m_0\Gamma_0(m)}, \tag{22}$$

where m_0 is the resonance mass, and $\Gamma_0(m)$ is defined as

$$\Gamma_0(m) = \Gamma_0 \frac{m_0}{m}\left(\frac{q}{q_0}\right). \tag{23}$$

The invariant amplitude $M_J(m)$ is proportional to $R_J(m)$:

$$M_J(m) \propto \frac{m}{q} R_J(m) \tag{24}$$

and can be expressed, for example, for $J = 0$, as

$$M_0(m) \propto \frac{m}{q\cot\Delta B - iq} + e^{2i\Delta B}\frac{\Gamma_0 m_0^2/q_0}{(m_0^2 - m^2) - im_0\Gamma_0(m)}. \tag{25}$$

The resulting $(K\pi)_0^{*0}$ invariant mass distribution is shown in Fig. 4, along with the phase and distributions for the other resonances. The mass parameters describing the three spin states in the m distribution are shown in Table IV. Measurements of the LASS experiment are used for the parameters of the $J = 0$ contribution and for the interaction radius [25,26]. The values of m_0, Γ_0, a, and b used in this analysis are different from those quoted in Ref. [25] due to better handling of the fit to the LASS data [26]. The two sets of values are consistent within errors and lead to similar results.

To account for the three-body kinematics in the analysis of $B^0 \to \varphi K\pi$ decays, we multiply the amplitude squared $|M_J(m)|^2$ by the phase-space factor $F(m)$:

$$F(m) = 2 \times m \times [m^2_{\rm max}(m) - m^2_{\rm min}(m)], \tag{26}$$

where $m^2_{\rm max}$ and $m^2_{\rm min}$ are the maximum and minimum values of the Dalitz plot range of $m^2_{\varphi K}$ ($m_{\varphi K}$ is the φK invariant mass) at any given value of $m_{K\pi}$; see the kinematics section of Ref. [18]. Because of slow dependence of the factor in Eq. (26) on m in any small range of m, the difference of this approach from the quasi-two-body approximation is small.

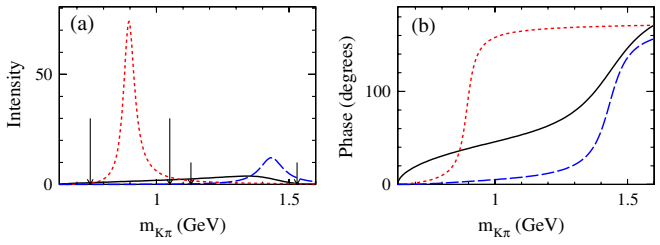

FIG. 4 (color online). Intensity $|M_J(m_{K\pi})|^2$ (a) and phase $\arg(M_J(m_{K\pi}))$ (b) of the invariant amplitudes for $J = 0$ (solid line), $J = 1$ (dashed line), and $J = 2$ (long-dashed line) $K\pi$ contributions as a function of the invariant $K\pi$ mass $m_{K\pi}$. The taller two arrows indicate the low $m_{K\pi}$ region, while the shorter two arrows indicate the high $m_{K\pi}$ region. The relative intensity of the amplitudes is taken from Fig. 2, while the absolute intensity is shown in arbitrary units.

TABLE IV. Parametrization of the $K\pi$ invariant mass distribution in the $B^0 \to \varphi(K\pi)_J$ decays where three resonance final states with spin $J = 0, 1, 2$ are considered. The resonance mass m_J, width Γ_J [18,25,26], interaction radius r, scattering length a, and effective range b are considered [25,26]. Combined errors are quoted, except for $(K\pi)_0^{*0}$ where the systematic errors are quoted last while the central values and statistical errors have been updated [26] with respect to Ref. [25].

	$(K\pi)_0^{*0}$ $J = 0$	$K^*(892)^0$ $J = 1$	$K_2^*(1430)^0$ $J = 2$
m_J (MeV)	$1435 \pm 5 \pm 5$	896.00 ± 0.25	1432.4 ± 1.3
Γ_J (MeV)	$279 \pm 6 \pm 21$	50.3 ± 0.6	109 ± 5
r (GeV^{-1})	...	3.4 ± 0.7	2.7 ± 1.3
a (GeV^{-1})	$1.95 \pm 0.09 \pm 0.06$	...	...
b (GeV^{-1})	$1.76 \pm 0.36 \pm 0.67$	...	...

C. Interference effects

The differential decay width discussed in Eq. (7) involves interference terms between resonances with different spins J. These interference terms have unique angular and mass dependences which cannot be factorized in the full distribution. We can parametrize the mass and angular amplitude for each spin state J as follows:

$$A_0(m_{K\pi}, \theta_1, \theta_2, \Phi) = Y_0^0(\mathcal{H}_1, \Phi)Y_1^0(-\mathcal{H}_2, 0)M_0(m_{K\pi})A_{00}, \tag{27}$$

$$A_1(m_{K\pi}, \theta_1, \theta_2, \Phi) = \sum_{\lambda=0,\pm1} Y_1^\lambda(\mathcal{H}_1, \Phi)Y_1^{-\lambda}(-\mathcal{H}_2, 0) \times M_1(m_{K\pi})A_{1\lambda}, \tag{28}$$

$$A_2(m_{K\pi}, \theta_1, \theta_2, \Phi) = \sum_{\lambda=0,\pm1} Y_2^\lambda(\mathcal{H}_1, \Phi)Y_1^{-\lambda}(-\mathcal{H}_2, 0) \times M_2(m_{K\pi})A_{2\lambda}. \tag{29}$$

The interference will appear in the angular-mass distributions as $2\Re e(A_i(m_{K\pi}, \theta_1, \theta_2, \Phi)A_j^*(m_{K\pi}, \theta_1, \theta_2, \Phi))$. As we can see from Fig. 4, the overlap between the P- and D-wave $K\pi$ contributions is negligibly small, and we will consider only the interference between the $J = 0$ and $J = 1$, or $J = 0$ and $J = 2$ amplitudes. The resulting two interference terms, properly normalized, are defined for $J = 1$ and $J = 2$:

$$\frac{2\Re e(A_J A_0^*)}{\sqrt{\Sigma|A_{J\lambda}|^2}|A_{00}|} = \sum_{i=7}^{9} \alpha_{iJ}^-(m_{K\pi}) f_{iJ}(\mathcal{H}_1, \mathcal{H}_2, \Phi), \tag{30}$$

where the angular dependence is defined in Table V, and $\alpha_{iJ}^-(m_{K\pi})$ are defined for $i = 7, 8, 9$ as

TABLE V. Parametrization of the angular distribution in Eq. (30). Interference between either $J = 0$ and $J = 1$, or $J = 0$ and $J = 2$, contributions in the $B^0 \to \varphi(K\pi)_J$ decays is considered. The common constant is quoted for each decay mode and is omitted from each individual function below. The three helicity angle parameters ($\mathcal{H}_1$, $\mathcal{H}_2$, Φ) are discussed in the text.

	$\varphi K^*(892)/\varphi(K\pi)^*_0$ $J = 1$	$\varphi K^*_2(1430)/\varphi(K\pi)^*_0$ $J = 2$
Common constant	$3\sqrt{3}/4\pi$	$3\sqrt{5}/8\pi$
$f_{7J}(\mathcal{H}_1, \mathcal{H}_2, \Phi)$	$\mathcal{H}_1\mathcal{H}_2^2$	$(3\mathcal{H}_1^2 - 1)\mathcal{H}_2^2$
$f_{8J}(\mathcal{H}_1, \mathcal{H}_2, \Phi)$	$\frac{1}{\sqrt{2}}\sqrt{1-\mathcal{H}_1^2}\sqrt{1-\mathcal{H}_2^2}\mathcal{H}_2\cos\Phi$	$\sqrt{6}\sqrt{1-\mathcal{H}_1^2}\mathcal{H}_1\sqrt{1-\mathcal{H}_2^2}\mathcal{H}_2\cos\Phi$
$f_{9J}(\mathcal{H}_1, \mathcal{H}_2, \Phi)$	$-\frac{1}{\sqrt{2}}\sqrt{1-\mathcal{H}_1^2}\sqrt{1-\mathcal{H}_2^2}\mathcal{H}_2\sin\Phi$	$-\sqrt{6}\sqrt{1-\mathcal{H}_1^2}\mathcal{H}_1\sqrt{1-\mathcal{H}_2^2}\mathcal{H}_2\sin\Phi$

$$\alpha^-_{7J}(m_{K\pi}) = \sqrt{f^-_{LJ}}\,\Re e(M_J(m_{K\pi})M^*_0(m_{K\pi})e^{-i\delta^-_{0J}}), \quad (31)$$

$$\alpha^-_{8J}(m_{K\pi}) = \sqrt{1-f^-_{LJ}-f^-_{\perp J}}\,\Re e(M_J(m_{K\pi})M^*_0(m_{K\pi}) \times e^{i\phi^-_{\|J}}e^{-i\delta^-_{0J}}), \quad (32)$$

$$\alpha^-_{9J}(m_{K\pi}) = \sqrt{f^-_{\perp J}}\,\Im m(M_J(m_{K\pi})M^*_0(m_{K\pi})e^{i\phi^-_{\perp J}}e^{-i\delta^-_{0J}}). \quad (33)$$

The above terms are specific to the B^0 decays and are denoted with superscript "$-$," as introduced in Eqs. (1)–(6). The interference distributions for the $\bar{B}^0$ decays are described by the same Eq. (30), but replacing A by $\bar{A}$ and α^-_{iJ} by α^+_{iJ} and with definitions given by Eqs. (31)–(33), replacing superscript "$-$" by "$+$."

The main difference now is that the $\alpha^-_{iJ}(m_{K\pi})$ parameters, as defined for $i = 7, 8, 9$, have a different dependence on mass to those defined for $i = 1$–6 in Eqs. (9)–(14). This dependence now includes the phase of the resonance amplitude as a function of mass. This dependence becomes crucial in resolving the phase ambiguities.

As can be seen from Eqs. (8)–(14), for any given set of values ($\phi_{\|J}$, $\phi_{\perp J}$, $\Delta\phi_{\|J}$, $\Delta\phi_{\perp J}$) a simple transformation of phases, for example, ($2\pi - \phi_{\|J}$, $\pi - \phi_{\perp J}$, $-\Delta\phi_{\|J}$, $-\Delta\phi_{\perp J}$), gives rise to another set of values that satisfy the above equations in an identical manner. This results in a fourfold ambiguity (twofold for each of B^0 and $\bar{B}^0$ decays). At any given value of $m_{K\pi}$ the distributions, including the interference terms in Eqs. (32) and (33), are still invariant under the above transformations if we flip the sign of the phase $\arg(M_J(m_{K\pi})M^*_0(m_{K\pi})e^{-i\delta^\pm_{0J}})$. At a given value of $m_{K\pi}$ this phase has to be determined from the data and we cannot resolve the ambiguity. However, the mass dependence of this phase is unique, given that the parameters $\delta^\pm_{0J}$ are constant. Therefore, the two ambiguous solutions for each B^0 and $\bar{B}^0$ decay can be fully resolved from the $m_{K\pi}$ dependence of the angular distributions in Eq. (30).

This technique of resolving the two ambiguous solutions in $B \to VV$ decays has been introduced in the analysis of $B^0 \to J/\psi K^{*0}$ decays [27] and has been used in *BABAR*'s earlier analysis of both $B \to \varphi K^{*0}$ and $\varphi K^{*\pm}$ decays [20,21]. It is based on Wigner's causality principle [28], where the phase of a resonant amplitude increases with increasing invariant mass; see Eq. (15). As a result, both the P-wave and D-wave resonance phase shifts increase rapidly in the vicinity of the resonance, while the corresponding S-wave increases only gradually, as seen in Fig. 4.

D. Time-dependent distributions

Measurement of the time-dependent CP asymmetry $\mathcal{A}(\Delta t)$ in the decay of a neutral B meson to a CP eigenstate, dominated by the tree-level $b \to c$ amplitude or by the penguin $b \to s$ amplitude, such as $B^0 \to (c\bar{c})K^0_S$ or $B^0 \to (s\bar{s})K^0_S$, where $(c\bar{c})$ and $(s\bar{s})$ are charmonium or quarkonium states, respectively, gives an approximation $\beta_{\rm eff}$ to the CKM unitarity triangle angle β [29]. The CP asymmetry is defined by

$$\mathcal{A}(\Delta t) = \frac{N(\Delta t, B^0_{\rm tag}) - N(\Delta t, \bar{B}^0_{\rm tag})}{N(\Delta t, B^0_{\rm tag}) + N(\Delta t, \bar{B}^0_{\rm tag})} = S\sin(\Delta m_B \Delta t) - C\cos(\Delta m_B \Delta t), \quad (34)$$

and

$$-\sin(2\beta_{\rm eff}) = \Im m\left(\frac{q}{p}\frac{\bar{A}}{A}\right)\Big/\left|\frac{q}{p}\frac{\bar{A}}{A}\right| = \eta_{CP} \times S/\sqrt{1-C^2}, \quad (35)$$

where $N(\Delta t, B^0_{\rm tag})$ or $N(\Delta t, \bar{B}^0_{\rm tag})$ is the number of events observed to decay at time Δt, in which the flavor of the B meson opposite to that of the decaying B at $\Delta t = 0$ (referred to as the flavor "tag") is known to be B^0 or $\bar{B}^0$, respectively, $\eta_{CP} = \pm 1$ is the CP eigenvalue of the final state; amplitudes A and $\bar{A}$ describe the direct decays of B^0 and $\bar{B}^0$ respectively to the final state; and Δm_B is the mixing frequency due to the difference in masses between the B meson eigenstates. We use a convention with $\bar{A} = \eta_{CP} \times A$ in the absence of CP violation. The above asymmetry follows from the time evolution of each flavor:

$$N(\Delta t, B^0_{\rm tag}) \propto \frac{e^{-|\Delta t|/\tau_B}}{4\tau_B}(1 + S\sin(\Delta m_B \Delta t) - C\cos(\Delta m_B \Delta t)), \quad (36)$$

$$N(\Delta t, \bar{B}^0_{\rm tag}) \propto \frac{e^{-|\Delta t|/\tau_B}}{4\tau_B}(1 - S\sin(\Delta m_B \Delta t) + C\cos(\Delta m_B \Delta t)). \quad (37)$$

The B^0-$\bar{B}^0$ mixing parameters q and p can be expressed to a good approximation using the Wolfenstein phase convention within the standard model [18]:

$$\arg\left(\frac{q}{p}\right) = -2\beta, \quad (38)$$

$$\left|\frac{q}{p}\right| = 1. \quad (39)$$

The value of $\sin 2\beta$ from the charmonium $b \to c$ decays, which defines the phase of the mixing diagram in the Wolfenstein parametrization, is well measured [3,18]:

$$\sin 2\beta = 0.681 \pm 0.025 \quad \text{or} \quad 2\beta = (0.75 \pm 0.03)\ \text{rad}, \quad (40)$$

where the phase ambiguity of β in the range $[0, \pi]$ has been resolved using vector-vector charmonium B decays [27] and the decay $B^0 \to K^+K^-K^0$ [30]. Should there be a new physics contribution to the mixing diagram, its effect is absorbed into the definition of β in Eq. (38), which should be valid for the analysis discussed in this paper. New physics effects in the $b \to c$ amplitude are unlikely to be significant as this transition is not suppressed in the standard model. Therefore the comparison of $\sin 2\beta$ in Eq. (40) with $\sin 2\beta_{\rm eff}$ measured in $b \to s$ transitions would be a test of new physics in the penguin B decays.

There is an alternative sign convention for the choice of the direct-CP violation parameter defined by

$$C = -\mathcal{A}_{CP} = \frac{|A|^2 - |\bar{A}|^2}{|A|^2 + |\bar{A}|^2}. \quad (41)$$

Given the approximation in Eq. (39) and our phase convention in Eq. (38), the value of S can be expressed as

$$S = \sqrt{1 - \mathcal{A}^2_{CP}} \times \sin\left(-2\beta + \arg\left(\frac{\bar{A}}{A}\right)\right). \quad (42)$$

Therefore, we have $S = -\eta_{CP} \times \sin 2\beta$ when $\bar{A} = \eta_{CP} \times A$. When we measure S in Eq. (42) with $b \to s$ decays, we can safely assume that the value of β has been measured in charmonium decays, as given in Eq. (40). Therefore, we are ultimately interested in the measurement of $\arg(\bar{A}/A)$. Any large deviation from $\arg(\eta_{CP})$ would be a signal of new physics.

In the study of the time evolution in Eq. (34) we can use the decay $B^0 \to \varphi(K^0_S\pi^0)^{*0}_0$ with an S-wave $K\pi$ contribution. This final state is a CP eigenstate with $\eta_{CP} = +1$ as we discuss below. However, the situation is more complicated in the general case of $B^0 \to \varphi K^0_S\pi^0$ decays where the final state is no longer a CP eigenstate. The amplitude for this decay is a superposition of CP eigenstates.

In Ref. [31] it was shown that the CP quantum numbers are independent of the $K^0_S\pi^0$ system, that is, independent of J, for the decay $B^0 \to (c\bar{c})K^0_S\pi^0$. The same analysis applies to $B^0 \to (s\bar{s})K^0_S\pi^0$. The CP parity is defined only by the $(s\bar{s})$ spin alignment λ (an alternative analysis that introduces the eigenstate of the transversity τ is sometimes used to separate the CP eigenstates [31]). For example, all longitudinal decays $B^0 \to \varphi K^0_S\pi^0$, corresponding to $\lambda = 0$, are CP-even, including the decay $B^0 \to \varphi(K^0_S\pi^0)^{*0}_0$. Overall, we conclude that in the decay $B^0 \to \varphi(K^0_S\pi^0)_J$ we have three amplitudes with definite CP:

$$A_{J0}, \qquad \eta_{CP} = +1, \quad (43)$$

$$A_{J\parallel} = (A_{J+} + A_{J-})/\sqrt{2}, \qquad \eta_{CP} = +1, \quad (44)$$

$$A_{J\perp} = (A_{J+} - A_{J-})/\sqrt{2}, \qquad \eta_{CP} = -1. \quad (45)$$

Similarly, $\eta_{CP} = -1$ for the B decay to the final state $f_0K^0_S\pi^0$, which will be considered as a background decay in our analysis. We do not discuss the CP properties of the interference terms with the product of amplitudes of different CP; these terms are integrated over in our analysis of the time evolution. These terms could be considered in a future experiment with higher statistics.

We can express the time-evolution coefficient in the decay $B^0 \to \varphi(K^0_S\pi^0)^{*0}_0$, as

$$S_{00} = -\sqrt{1 - \mathcal{A}^2_{00}} \times \sin(2\beta + 2\Delta\phi_{00}), \quad (46)$$

where $\mathcal{A}_{00} = \mathcal{A}_{CP0}$. For the decays $B^0 \to \varphi(K^0_S\pi^0)$ with $K^*(892)^0$ $(J = 1)$ or $K^*_2(1430)^0$ $(J = 2)$ intermediate resonances there are three time-evolution terms, one for each amplitude, if we ignore the interference terms:

$$S_{J0} = -\sqrt{1 - \mathcal{A}^2_{J0}} \times \sin(2\beta + 2\Delta\delta_{0J} + 2\Delta\phi_{00}), \quad (47)$$

$$S_{J\parallel} = -\sqrt{1 - \mathcal{A}^2_{J\parallel}} \times \sin(2\beta + 2\Delta\delta_{0J} - 2\Delta\phi_{\parallel J} + 2\Delta\phi_{00}), \quad (48)$$

$$S_{J\perp} = +\sqrt{1 - \mathcal{A}^2_{J\perp}} \times \sin(2\beta + 2\Delta\delta_{0J} - 2\Delta\phi_{\perp J} + 2\Delta\phi_{00}). \quad (49)$$

The three corresponding direct-CP violation terms $\mathcal{A}_{J0}$, $\mathcal{A}_{J\parallel}$, and $\mathcal{A}_{J\perp}$ can be obtained from the direct-CP violation and polarization parameters measured in the $\overset{(-)}{B}{}^0 \to \varphi(K^\pm\pi^\mp)$ decays:

$$\mathcal{A}_{J0} = \frac{\mathcal{A}_{CPJ} + \mathcal{A}^0_{CPJ}}{1 + \mathcal{A}_{CPJ} \times \mathcal{A}^0_{CPJ}}, \tag{50}$$

$$\mathcal{A}_{J\perp} = \frac{\mathcal{A}_{CPJ} + \mathcal{A}^\perp_{CPJ}}{1 + \mathcal{A}_{CPJ} \times \mathcal{A}^\perp_{CPJ}}, \tag{51}$$

$$\mathcal{A}_{J\parallel} = \frac{\mathcal{A}_{CPJ} - f_{LJ} \times (\mathcal{A}_{CPJ} + \mathcal{A}^0_{CPJ}) - f_{\perp J} \times (\mathcal{A}_{CPJ} + \mathcal{A}^\perp_{CPJ})}{1 - f_{LJ} \times (1 + \mathcal{A}_{CPJ} \times \mathcal{A}^0_{CPJ}) - f_{\perp J} \times (1 + \mathcal{A}_{CPJ} \times \mathcal{A}^\perp_{CPJ})}. \tag{52}$$

As can be seen from Eqs. (46)–(52), there is only one parameter $\Delta\phi_{00}$ that is not measurable in the $\overset{(-)}{B}{}^0 \to \varphi(K^\pm\pi^\mp)$ decays. Therefore, the above parametrization allows us to measure $\Delta\phi_{00}$ from the time evolution of the $B^0 \to \varphi(K^0_S\pi^0)$ decays while all other parameters are measured in the mode $\overset{(-)}{B}{}^0 \to \varphi(K^\pm\pi^\mp)$, which has a significantly larger reconstructed yield.

The angular distributions in Eq. (7) can be simplified after integrating over the angle Φ. The resulting angular distribution will not have interference terms between different amplitudes for a given J. This makes the time-evolution parametrization relatively simple with just two terms: longitudinal (f_{LJ}) and transverse ($1 - f_{LJ}$) polarization. The longitudinal time evolution is parametrized by the S_{J0} coefficient, and the transverse time evolution is parametrized by the expression

$$S_{JT} = \frac{f_{\perp J} \times (1 + \mathcal{A}_{CPJ} \times \mathcal{A}^\perp_{CPJ})}{1 - f_{LJ} \times (1 + \mathcal{A}_{CPJ} \times \mathcal{A}^0_{CPJ})} \times \mathcal{S}_{J\perp} + \left(1 - \frac{f_{\perp J} \times (1 + \mathcal{A}_{CPJ} \times \mathcal{A}^\perp_{CPJ})}{1 - f_{LJ} \times (1 + \mathcal{A}_{CPJ} \times \mathcal{A}^0_{CPJ})}\right) \times \mathcal{S}_{J\parallel}. \tag{53}$$

In a similar manner, the longitudinal direct CP-violation term is parametrized by the $C_{J0} = -\mathcal{A}_{J0}$ coefficient, and the transverse direct CP-violation term is parametrized by

$$C_{JT} = -\frac{f_{\perp J} \times (1 + \mathcal{A}_{CPJ} \times \mathcal{A}^\perp_{CPJ})}{1 - f_{LJ} \times (1 + \mathcal{A}_{CPJ} \times \mathcal{A}^0_{CPJ})} \times \mathcal{A}_{J\perp} - \left(1 - \frac{f_{\perp J} \times (1 + \mathcal{A}_{CPJ} \times \mathcal{A}^\perp_{CPJ})}{1 - f_{LJ} \times (1 + \mathcal{A}_{CPJ} \times \mathcal{A}^0_{CPJ})}\right) \times \mathcal{A}_{J\parallel}. \tag{54}$$

As an example, let us consider the $J = 1$ case. Since $A_{1\perp}$ and $A_{1\parallel}$ have opposite CP parity and it has been measured that $f_{\perp 1} \simeq f_{\parallel 1} \equiv (1 - f_{\perp 1} - f_{L1})$ [14,15,20], in the standard model we expect to a good approximation $S_{1T} \simeq 0$, $S_{10} = \sin 2\beta$, and $C_{1T} = C_{10} = 0$.

III. EVENT RECONSTRUCTION

We use a sample of $(465.0 \pm 5.1) \times 10^6$ $e^+e^- \to \Upsilon(4S) \to B\bar{B}$ events collected with the *BABAR* detector [32] at the PEP-II e^+e^- asymmetric-energy storage rings. The center-of-mass system of the $\Upsilon(4S)$ resonance is boosted providing roughly 250 μm average separation between the two B meson decay vertices. The e^+e^- center-of-mass energy $\sqrt{s}$ is equal to 10.58 GeV, corresponding to the $\Upsilon(4S)$ resonance.

We fully reconstruct the $\overset{(-)}{B}{}^0 \to \varphi(1020)\overset{(-)}{K}{}^{*0} \to (K^+K^-)(\overset{(-)}{K}\pi)$ candidates with two $(K\pi)$ final states $K^0_S\pi^0$ and $K^\pm\pi^\mp$. The neutral pseudoscalar mesons are reconstructed in the final states $K^0_S \to \pi^+\pi^-$ and $\pi^0 \to \gamma\gamma$. The dominant background in our analysis comes from $e^+e^- \to q\bar{q}$ production ($q = u, d, s, c$). A data sample equivalent in luminosity to 12% of the on-$\Upsilon(4S)$-resonance sample has been collected with $\sqrt{s}$ 40 MeV below the $\Upsilon(4S)$ resonance (off-resonance data) for studies of this background. A detailed GEANT4-based Monte Carlo (MC) simulation [33] of the detector has been used to model all processes. This simulation has been extensively tested and tuned with high-statistics validation samples.

Momenta of charged particles are measured in a tracking system consisting of a silicon vertex tracker (SVT) with five double-sided layers and a 40-layer drift chamber, both within the 1.5-T magnetic field of a solenoid. Identification of charged particles (PID) is provided by measurements of the energy loss in the tracking devices (dE/dx) and by a ring-imaging Cherenkov detector (DIRC). Photons are detected by a CsI(Tl) electromagnetic calorimeter (EMC). We use minimal information from the muon identification system (IFR) to make a loose veto of the charged muon tracks.

We require all charged-particle tracks (except for those from the $K^0_S \to \pi^+\pi^-$ decay) used in reconstructing the B candidate to originate from within 1.5 cm in the x-y plane and 10 cm in the z direction from the nominal beam spot. We veto leptons from our charged-particle track samples by demanding that tracks have DIRC, EMC, and IFR signatures that are inconsistent with either electrons or muons. Further pion and kaon PID requirements are based on a likelihood selection developed from dE/dx and Cherenkov angle information from the tracking detectors and DIRC, respectively. The typical efficiency of PID requirements is greater than 95% for charged tracks in our final states. Photons are reconstructed from energy

deposits in the electromagnetic calorimeter that are not associated with a charged track. We require that all photon candidates have an energy greater than 30 MeV in the EMC.

The invariant mass of the candidate K^0_S is required to lie within the range $|m_{\pi^+\pi^-} - m_{K^0}| < 12$ MeV. We perform a vertex-constrained fit to require that the two tracks originate from a common vertex and require that the lifetime significance of the K^0_S be $\tau/\sigma_\tau > 5$, where τ and σ_τ are the K^0_S lifetime and its uncertainty, respectively, determined from the vertex-constrained fit. For the K^0_S candidates, we also require the cosine of the angle between the flight direction from the interaction point and momentum direction to be greater than 0.995. The efficiency of K^0_S selection requirements is about 90%.

We select neutral-pion candidates from two photon clusters with the requirement that the $\gamma\gamma$ invariant mass satisfy $120 < m_{\gamma\gamma} < 150$ MeV. The mass of a π^0 candidate meeting this criterion is then constrained to the nominal value [18] and, when combined with other tracks or neutrals to form a B candidate, to originate from the B candidate vertex. This procedure improves the mass and energy resolution of the parent particle. The purity of K^0_S and π^0 selection is 92% (88%) and 90% (68%), respectively, in the signal sample (combinatorial background) based on MC simulation studies.

We identify B meson candidates using two main kinematic variables, beam energy-substituted mass $m_{\rm ES}$:

$$m_{\rm ES} = [(s/2 + \mathbf{p}_\Upsilon \cdot \mathbf{p}_B)^2/E^2_\Upsilon - \mathbf{p}^2_B]^{1/2}, \qquad (55)$$

and the energy difference ΔE:

$$\Delta E = (E_\Upsilon E_B - \mathbf{p}_\Upsilon \cdot \mathbf{p}_B - s/2)/\sqrt{s}, \qquad (56)$$

where $(E_B, \mathbf{p}_B)$ is the four-momentum of the B candidate and $(E_\Upsilon, \mathbf{p}_\Upsilon)$ is the e^+e^- initial-state four-momentum, both in the laboratory frame. Both variables are illustrated in Fig. 5. The distribution of ΔE is expected to peak at zero and $m_{\rm ES}$ at the B mass around 5.280 GeV. The ΔE resolution is dominated by the decay product energy and momentum measurements and is typically 34 and 20 MeV for the subchannels with and without a π^0, respectively. The typical $m_{\rm ES}$ resolution is 2.6 MeV and is dominated by the beam energy uncertainties. We require $m_{\rm ES} > 5.25$ GeV and $|\Delta E| < 100$ MeV to retain sidebands for later fitting of parameters to describe the backgrounds.

The requirements on the invariant masses of the resonances are $0.99 < m_{K\bar{K}} < 1.05$ GeV and $0.75 < m_{K^0_S\pi^0} < 1.55$ GeV, $0.75 < m_{K^\pm\pi^\mp} < 1.05$ GeV, or $1.13 < m_{K^\pm\pi^\mp} < 1.53$ GeV for the φ and K^{*0}, respectively. Here we separate the $K^\pm\pi^\mp$ invariant mass into two ranges for later fitting. The two ranges simplify the fit configuration and allow us to test the nonresonant $B \to \varphi K\pi$ contribution independently, therefore providing an independent cross-check of the parametrization.

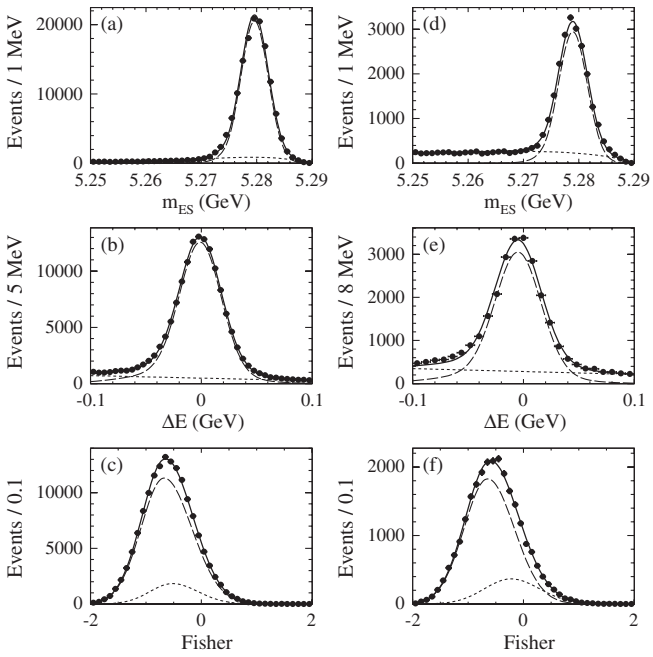

FIG. 5. Validation of kinematic variables with the high-statistics sample of $B^0 \to D^-\pi^+ \to (K^+\pi^-\pi^-)(\pi^+)$ decays. Projections onto the variables $m_{\rm ES}$, ΔE, and $\mathcal{F}$ are shown from top to bottom for MC (a)–(c) and data (d)–(f). The dots with error bars represent the MC simulation (left) or data (right). The long-dashed lines represent the signal and the solid lines show signal-plus-background parametrization. A small fraction of combinatorial background is present (dashed lines) due to combinations of other B decays in the MC and also $q\bar{q}$ continuum in the data.

To reject the dominant $e^+e^- \to q\bar{q}$ background, we use variables calculated in the center-of-mass frame. We require $|\cos\theta_T| < 0.8$, where θ_T is the angle between the B-candidate thrust axis and that of the rest of the event. The angle θ_T is the most powerful of the event-shape variables we employ. The distribution of $|\cos\theta_T|$ is sharply peaked near 1 for combinations drawn from jetlike $q\bar{q}$ pairs and is nearly uniform for the isotropic B-meson decays. Further use of the event topology is made via the construction of a Fisher discriminant $\mathcal{F}$, which is subsequently used as a discriminating variable in the likelihood fit.

Our Fisher discriminant is an optimized linear combination of the remaining event-shape information, excluding $\cos\theta_T$. The variables entering the Fisher discriminant are the angles with respect to the beam axis of the B momentum and B thrust axis, and the zeroth and second angular moments $L_{0,2}$ of the energy flow about the B thrust axis, all calculated in the $\Upsilon(4S)$ center-of-mass frame. The moments are defined by

$$L_j = \sum_i p_i \times |\cos\theta_i|^j, \qquad (57)$$

where θ_i is the angle with respect to the B thrust axis of track or neutral cluster i, p_i is its momentum, and the sum

excludes the B candidate. The coefficients used to combine these variables are chosen to maximize the separation (difference of means divided by quadrature sum of errors) between the signal and continuum background distributions of L_j and are determined from studies of signal MC and off-peak data. We have studied the optimization of $\mathcal{F}$ for a variety of signal modes and find that the optimal sets of coefficients are nearly identical for all. Because the information contained in $\mathcal{F}$ is correlated with $|\cos\theta_T|$, the separation between signal and background is dependent on the $|\cos\theta_T|$ requirement made prior to the formation of $\mathcal{F}$. The $\mathcal{F}$ variable is illustrated in Fig. 5.

In order to establish that the MC simulation reproduces the kinematic observables in the data, such as $m_{\rm ES}$, ΔE, and $\mathcal{F}$, we use high-statistics B^0-meson decays with similar kinematics and topology. For example, in Fig. 5 we illustrate reconstructed $B^0 \to D^- \pi^+ \to (K^+\pi^-\pi^-)(\pi^+)$ decays. There is good agreement between data and MC. The deviations in the means of the distributions are about 0.7 MeV for $m_{\rm ES}$, 5 MeV for ΔE, and negligible for $\mathcal{F}$. We take these corrections into account when we study the $B^0 \to \varphi K\pi$ decays.

The B background contribution is generally found to be small due to selection on the narrow φ resonance, PID requirements on the kaons, and good momentum resolution, important, in particular, for ΔE. We remove $\overset{(-)}{B}{}^0 \to \varphi K^\pm \pi^\mp$ signal candidates that have decay products with invariant masses within 12 MeV of the nominal mass values for $D_s^\pm$ or $D^\pm$. This removes the background from the $B \to D_s^\pm K$, $D^\pm K$, $D_s^\pm \pi$, and $D^\pm \pi$ decays. To reduce combinatorial background in the $B^0 \to \varphi K_S^0 \pi^0$ analysis with low-momentum π^0 candidates, we require $\mathcal{H}_1 < 0.8$. Certain types of B background, such as potential $B^0 \to f_0(980)K\pi$, cannot be distinguished on an event-by-event basis, and so cannot be removed by vetoes. We incorporate these contributions into the fit. The remaining B background events were found to be random combinations of tracks and can be treated as combinatorial background, similar to random tracks from $q\bar{q}$ production.

When more than one candidate is reconstructed, which happens in 5% of $\varphi K^\pm \pi^\mp$ and 10% of $\varphi K_S^0 \pi^0$ events, we select one candidate per event based on the lowest value of the χ^2 of the four-track vertex for $\overset{(-)}{B}{}^0 \to \varphi K^\pm \pi^\mp$ or of the fitted $\overset{(-)}{B}{}^0 \to \varphi K_S^0 \pi^0$ decay tree.

In the self-tagging B-decay mode $\overset{(-)}{B}{}^0 \to \varphi K^\pm \pi^\mp$, we define the b-quark flavor sign Q to be opposite to the charge of the kaon candidate. For each reconstructed $\overset{(-)}{B}{}^0 \to \varphi K_S^0 \pi^0$ signal candidate ($B_{\rm sig}$) we use the remaining tracks in the event to determine the decay vertex position and flavor of the other B decay $B_{\rm tag}$. A neural network based on kinematic and particle identification information assigns each event to one of seven mutually exclusive tagging categories ($c_{\rm tag}$) [34], including a category for events in which a tag flavor is not determined. The B-flavor-tagging algorithm is trained to identify primary leptons, kaons, soft pions, and high-momentum charged particles from the other B and correlate this information to the B flavor. The performance of this algorithm is evaluated using a data sample ($B_{\rm flav}$ sample) of fully reconstructed $B^0 \to D^{(*)-}\pi^+/\rho^+/a_1^+$ decays. The effective tagging efficiency is measured to be $(31.2 \pm 0.3)\%$.

We determine the proper time difference Δt between $B_{\rm sig}$ and $B_{\rm tag}$ from the spatial separation between their decay vertices. The $B_{\rm tag}$ vertex is reconstructed from the remaining charged tracks in the event, and its uncertainty dominates the Δt resolution $\sigma_{\Delta t}$. The average proper time resolution is $\langle\sigma_{\Delta t}\rangle \approx 0.7$ ps. Only events that satisfy $|\Delta t| < 15$ ps and $0.1 < \sigma_{\Delta t} < 2.5$ ps are retained.

Overall, selection requirements discussed here have been optimized to retain large signals and wide sidebands of observables for later fitting, as discussed in the next section. Statistical precision of the measurements was the main optimization factor, while individual systematic uncertainties were kept small compared to statistical errors. After applying all selection criteria and using the measured branching fractions summarized in Table I, we expect to observe about 177 (15) $\overset{(-)}{B}{}^0 \to \varphi(\overset{(-)}{K}\pi)_0^{*0}$, 473 (34) $\overset{(-)}{B}{}^0 \to \varphi\overset{(-)}{K}{}^*(892)^0$, and 156 (9) $\overset{(-)}{B}{}^0 \to \varphi\overset{(-)}{K}{}_2^*(1430)^0$ events in the $\varphi K^\pm\pi^\mp$ ($\varphi K_S^0\pi^0$) channel. The larger reconstruction efficiency and secondary branching fractions in the $\varphi K^\pm\pi^\mp$ channel result in the dominance of this decay mode in the signal parameter measurements, except for the measurement of the $\Delta\phi_{00}$ parameter, which is possible only with the $\varphi K_S^0\pi^0$ channel.

IV. ANALYSIS METHOD

We use an unbinned, extended maximum-likelihood (ML) fit [14] to extract the 27 parameters defined in Table II, which describe three decay channels [twelve in either $B^0 \to \varphi K^*(892)^0$ or $\varphi K_2^*(1430)^0$, and three in $\varphi(K\pi)_0^{*0}$ decays]. We perform a joint fit to the data for three modes: $\varphi K_S^0\pi^0$; $\varphi K^\pm\pi^\mp$ in the lower $K\pi$ mass range (0.75–1.05 GeV) and $\varphi K^\pm\pi^\mp$ in the higher $K\pi$ mass range (1.13–1.53 GeV). To simplify treatment of the likelihood function, we separate the two ranges of the $K^\pm\pi^\mp$ invariant mass. However, in the joint fit the likelihood function $\mathcal{L}$ is written as a product of three independent likelihood functions, one for each of the above three modes, as discussed below.

Because of the relatively low statistics, we simplify the angular analysis in the $B^0 \to \varphi K_S^0\pi^0$ decay mode. We integrate the angular distributions in Eq. (7) over the angle Φ. Therefore only the longitudinal polarization fractions f_{LJ}, the yields, and the time evolution are measured with the $B^0 \to \varphi K_S^0\pi^0$ decays. We constrain the relative signal yields for the same spin-J contributions in the two subchannels $\varphi(K^\pm\pi^\mp)_J$ and $\varphi(K_S^0\pi^0)_J$ taking into account the

isospin relationship, daughter branching fractions, and reconstruction efficiency corrections. The isospin relationship requires that the $K^{*0} \to K^+\pi^-$ and $K^0\pi^0$ fractions are $2/3$ and $1/3$ of the total $K\pi$ decay rate, respectively, and we ignore any isospin violation as being negligible for the measurements in this analysis. All other signal parameters in Table II are constrained to be the same when they appear in both channels.

A. Likelihood function

The likelihood function for $B^0 \to \varphi K^0_S\pi^0$ is written as

$$\mathcal{L} = \prod_c \exp(-N_c) \prod_i^{N_c} \Big(\sum_j n_j f_j^c \mathcal{P}_j^c(\vec{x}_i; \vec{\zeta}; \vec{\xi}) \Big), \qquad (58)$$

where n_j is the unconstrained (except if noted otherwise) number of events for each event type j, f_j^c is the fraction of events of component j for each tagging category c, $N_c = \sum_j f_j^c n_j$ is the number of events found by the fit for tagging category c, and $\mathcal{P}_j^c(\vec{x}_i; \vec{\zeta}; \vec{\xi})$ is the probability density function (PDF).

The data model has five event types j: the signal $B^0 \to \varphi(K\pi)_J$ with $J = 0, 1, 2$, a possible background from $B^0 \to f_0(980)K^{*0}$, and combinatorial background. The combinatorial background PDF is found to account well for both the dominant light $q\bar{q}$ events and the random tracks from B decays. Each event candidate i is characterized by a set of 10 observables $\vec{x}_i = \{m_{\rm ES}, \Delta E, \mathcal{F}, m_{K\pi}, m_{K\bar{K}}, \mathcal{H}_1, \mathcal{H}_2, c_{\rm tag}, \Delta t, \sigma_{\Delta t}\}_i$, the kinematic observables $m_{\rm ES}$, ΔE, and $\mathcal{F}$, the K^* and φ invariant masses $m_{K\pi}$ and $m_{K\bar{K}}$, the helicity angles $\mathcal{H}_1$ and $\mathcal{H}_2$, the flavor tag $c_{\rm tag}$, the proper time difference Δt and its event-by-event error $\sigma_{\Delta t}$. The PDFs are split into the seven tagging categories. The polarization parameters quoted in Table II are denoted by $\vec{\zeta}$ and the remaining parameters by $\vec{\xi}$. Most of the $\vec{\zeta}$ parameters, except for $\Delta\phi_{00}$, appear also in the likelihood function for the $\overset{(-)}{B}{}^0 \to \varphi K^\pm\pi^\mp$ decays.

The likelihood function for $\overset{(-)}{B}{}^0 \to \varphi K^\pm\pi^\mp$ decays, in either the lower or the higher $K\pi$ mass range, is

$$\mathcal{L} = \exp\Big(-\sum_j n_j\Big) \prod_i \Big(\sum_{j,k} n_j^k \mathcal{P}_j^k(\vec{x}_i; \mu^k, \vec{\zeta}, \vec{\xi}) \Big), \qquad (59)$$

where the index j represents the three event types used in our data model: the signal $B^0 \to \varphi(K\pi)^0$ ($j = 1$) which combines the two dominant modes in a given mass range [$\varphi K^*(892)^0$ and $\varphi(K\pi)^{*0}_0$ in the lower or $\varphi K^*_2(1430)^0$ and $\varphi(K\pi)^{*0}_0$ in the higher mass range], a possible background from $B^0 \to f_0(980)K^{*0}$ ($j = 2$), and a combinatorial background ($j = 3$). The superscript k corresponds to the value of the flavor sign $Q = \pm 1$ and allows for a CP-violating difference between the B^0 and $\bar{B}^0$ decay amplitudes (A and $\bar{A}$).

In the signal event type, the yield and asymmetry $n_{\rm sig}$ and $\mathcal{A}_{CP}$, respectively, of the $\overset{(-)}{B}{}^0 \to \varphi(K^\pm\pi^\mp)_J$ mode with $J = 1$ in the lower mass range or $J = 2$ in the higher mass range and those of the $\overset{(-)}{B}{}^0 \to \varphi(K^\pm\pi^\mp)^{*0}_0$ mode are parametrized by applying the fraction μ^k of the $\varphi(K\pi)_J$ yield to n_1^k. Hence, $n_{\rm sig} = n_1^+ \times \mu^+ + n_1^- \times \mu^-$, $\mathcal{A}_{CP} = (n_1^+ \times \mu^+ - n_1^- \times \mu^-)/n_{\rm sig}$, and the $\varphi(K^\pm\pi^\mp)^{*0}_0$ yield is $n_1^+ \times (1 - \mu^+) + n_1^- \times (1 - \mu^-)$. This treatment is necessary to include interference between the two decay modes as we discuss below, while we ignore interference in the $B^0 \to \varphi K^0_S\pi^0$ channel due to low statistics. The PDF is formed from the following set of observables: $\vec{x}_i = \{m_{\rm ES}, \Delta E, \mathcal{F}, m_{K\pi}, m_{K\bar{K}}, \mathcal{H}_1, \mathcal{H}_2, \Phi, Q\}$, and the dependence on μ^k and polarization parameters $\vec{\zeta} \equiv \{f_{LJ}, f_{\perp J}, \phi_{\|J}, \phi_{\perp J}, \delta_{0J}, \mathcal{A}^0_{CPJ}, \mathcal{A}^\perp_{CPJ}, \Delta\phi_{\|J}, \Delta\phi_{\perp J}, \Delta\delta_{0J}\}$ is relevant only for the signal PDF $\mathcal{P}_1^k$.

The remaining PDF parameters $\vec{\xi}$, in both the $\overset{(-)}{B}{}^0 \to \varphi K^0_S\pi^0$ and the $\varphi K^\pm\pi^\mp$ channels, are left free to vary in the fit for the combinatorial background and are fixed to the values extracted from MC simulation and calibration $B \to \bar{D}\pi$ decays for the other event types. We minimize the $-2\ln\mathcal{L}$ function using MINUIT [35] in the ROOT framework [36]. The statistical error on a parameter is given by its change when the quantity $-2\ln\mathcal{L}$ increases by one unit. The statistical significance is taken as the square root of the difference between the value of $-2\ln\mathcal{L}$ for zero signal and the value at its minimum. We have tested this procedure with simulated samples and found good agreement with the statistical expectations.

B. PDF parametrization

The PDF $\mathcal{P}_j^k(\vec{x}_i; \mu^k, \vec{\zeta}; \vec{\xi})$ for a given $\overset{(-)}{B}{}^0 \to \varphi K^\pm\pi^\mp$ or $\varphi K^0_S\pi^0$ candidate i is taken to be a joint PDF for the helicity angles, resonance masses, and Q and the product of the PDFs for each of the remaining variables. The assumption of negligible correlations in the selected data sample among the discriminating variables, except for resonance masses and helicity angles where relevant, has been validated by evaluating the correlation coefficients. This assumption was further tested with the MC simulation.

For the parametrization of the signal PDFs we use double-Gaussian functions for signal ΔE and $m_{\rm ES}$. For the background we use low-degree polynomials as required by the data or, in the case of $m_{\rm ES}$, an empirical threshold ARGUS function [37]:

$$f(x) \propto x\sqrt{1 - x^2}\exp[-\xi_1(1 - x^2)], \qquad (60)$$

where $x \equiv m_{\rm ES}/E_{\rm beam}$ and ξ_1 is a parameter that is determined from the fit with a typical value of about 25.

For both signal and background, the Fisher distribution $\mathcal{F}$ is described well by a Gaussian function with different

widths to the left and right of the mean. For the combinatorial background distribution, we also include a second Gaussian function with a larger width to account for a small tail in the signal $\mathcal{F}$ region. This additional component of the PDF is important, because it prevents the background probability from becoming too small in the region where signal lies.

A relativistic spin-J B-W amplitude parametrization is used for the resonance masses [18,38], except for the $(K\pi)_0^{*0}$ $m_{K\pi}$ amplitude, which is parametrized with the LASS function [25,26]. The latter includes the $K_0^*(1430)^0$ resonance together with a nonresonant component. The detailed treatment of the invariant mass distribution is discussed in Sec. II B. We found that no additional correction to the $K\pi$ invariant mass parametrization is necessary because resolution effects of only a few MeV are negligibly small compared with the resonance widths. On the other hand, we convolve resolution effects into the $m_{K\bar{K}}$ parametrization.

The background parametrizations for candidate masses include resonant components to account for resonance production in the background. The background shape for the helicity parametrization is also separated into contributions from combinatorial background and from real mesons, both fit by low-degree polynomials.

The mass-helicity PDF is the ideal distribution from Eqs. (27)–(30), multiplied by an empirically determined acceptance function $\mathcal{G}(\mathcal{H}_1, \mathcal{H}_2, \Phi) \equiv \mathcal{G}_1(\mathcal{H}_1) \times \mathcal{G}_2(\mathcal{H}_2)$, which is a parametrization of the relative reconstruction efficiency as a function of helicity angles. It was found with detailed MC simulation that resolution effects in the helicity angles introduce negligible effects in the PDF parametrization and fit performance, and they are therefore ignored. The angles between the final-state particles and their parent resonances are related to their momenta. The signal acceptance effects parametrized with the function $\mathcal{G}(\mathcal{H}_1, \mathcal{H}_2, \Phi)$ are due to kinematic correlations, whereas the detector geometry correlations are negligible. Therefore the above uncorrelated parametrization as a function of two helicity angles was found to be appropriate and was validated with detailed MC simulation.

Momentum in the laboratory frame is strongly correlated with detection efficiency. Thus we have acceptance effects in the helicity observables $\mathcal{H}_i$, most evident for the large values of $\mathcal{H}_1$ corresponding to the slow π from the K^* meson. However, these acceptance effects are not present for the Φ angle; there is no correlation with the actual direction with respect to the detector, which is random for the B decays. The acceptance effects for the two helicity angles $\mathcal{H}_1$ and $\mathcal{H}_2$ are shown in Fig. 6. We obtain the acceptance functions from the fit to the signal MC helicity distribution, with the known relative components of longitudinal and transverse amplitudes generated with $B^0 \to \varphi K^*(892)^0$ MC. The $D_{(s)}^{\pm}$-meson veto causes the sharp acceptance dips around 0.8 in the $\mathcal{G}_1(\mathcal{H}_1)$ function in the $\overset{(-)}{B}{}^0 \to \varphi K^{\pm}\pi^{\mp}$ analysis.

The interference between the $J = 1$ or $J = 2$ and the S-wave $(K\pi)$ contributions is modeled with the term $2\Re e(A_J A_0^*)$ in Eq. (30) with the four-dimensional angular and $m_{K\pi}$ dependence, as discussed in detail in Sec. II C. It has been shown in the decays $B^0 \to J/\psi(K\pi)_0^{*0}$ and $B^{\pm} \to \pi^{\pm}(K\pi)_0^{*0}$ [27] that the amplitude behavior as a function of $m_{K\pi}$ is consistent with that observed by LASS except for a constant phase shift. Integrating the probability distribution over $(\mathcal{H}_1, \mathcal{H}_2, \Phi)$, the interference term $2\Re e(A_J A_0^*)$ should vanish. However, as we introduce the detector acceptance effects on $(\mathcal{H}_1, \mathcal{H}_2)$, the interference contribution becomes nonzero. The total yield of the two modes is corrected before calculating the branching fractions. The effect can be estimated by comparing the integral of $B^0 \to \varphi K_2^*(1430)^0$, $B^0 \to \varphi(K\pi)_0^{*0}$ and the interference probability contribution. We find that the interference term accounts for 3.5% of the total yield. Accordingly, we scale the yields of $B^0 \to \varphi K_2^*(1430)^0$ and $B^0 \to \varphi(K\pi)_0^{*0}$ modes by 96.5% while calculating the branching fraction. This effect is negligible for the $B^0 \to \varphi K^*(892)^0$ decay due to the relatively small fraction of the $B^0 \to \varphi(K\pi)_0^{*0}$ contribution to the lower $K\pi$ mass range.

The parametrization of the nonresonant signal-like contribution $B^0 \to f_0 K^{*0} \to (K^+K^-)K^{*0}$ is identical to the signal in the primary kinematic observables $m_{\rm ES}$, ΔE, $\mathcal{F}$, and the $m_{K\pi}$ mass but is different in the angular and $m_{K\bar{K}}$ distributions. For $B^0 \to f_0 K^{*0}$, the ideal angular distribution is uniform in Φ and $\mathcal{H}_2$ and is proportional to $\mathcal{H}_1^2$, due to angular momentum conservation. We use a coupled-channel B-W function to model the K^+K^- mass distribu-

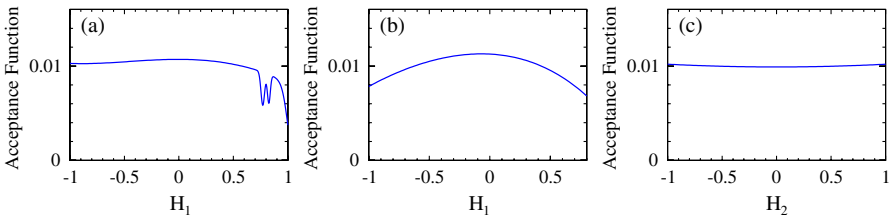

FIG. 6 (color online). Angular acceptance functions for $\mathcal{H}_1$ in $\varphi K^{\pm}\pi^{\mp}$ (a), in $\varphi K_S^0\pi^0$ (b), and for $\mathcal{H}_2$ (c). These plots show only relative efficiency between different helicity points with arbitrary y-axis units. The $D_{(s)}^{\pm}$-meson veto causes the sharp acceptance dips near $\mathcal{H}_1 = 0.8$ seen in (a).

tion for the f_0 [38]. The broad invariant mass distribution of f_0 compared to the narrow φ resonance was found to account well for any broad $m_{K\bar{K}}$ contribution. This PDF parametrization is further varied as part of the systematic uncertainty studies. The $m_{K\pi}$ distribution in $B^0 \to f_0 K^{*0}$ is parametrized as a $J = 1$ contribution in the lower mass range and as a $J = 0$ contribution in the higher mass range; see Sec. II B.

For the $B^0 \to \varphi K^0_S \pi^0$ mode, the Φ angle is integrated over, so that no interference terms appear in the fit. An additional PDF for the Δt distribution is used for both the signal and the background, which is discussed next. The treatment of other observables is similar to those of $\overset{(-)}{B}{}^0 \to \varphi K^{\pm}\pi^{\mp}$.

Time-dependent CP asymmetries are determined using the difference of B^0 meson proper decay times $\Delta t \equiv t_{\rm sig} - t_{\rm tag}$, where $t_{\rm sig}$ is the proper decay time of the signal B ($B_{\rm sig}$) and $t_{\rm tag}$ is that of the other B ($B_{\rm tag}$). The Δt distribution for $B_{\rm sig}$ decaying to a CP eigenstate

$$f(\Delta t, Q_{\rm tag}) \sim \frac{e^{-|\Delta t|/\tau_B}}{4\tau_B}\{1 - Q_{\rm tag}\Delta w + Q_{\rm tag}\mu(1-2w) + (Q_{\rm tag}(1-2w) + \mu(1 - Q_{\rm tag}\Delta w)) \times [S\sin(\Delta m_B \Delta t) - C\cos(\Delta m_B \Delta t)]\} \quad (61)$$

is convolved with a resolution function $\mathcal{R}$. The parameter $Q_{\rm tag} = +1(-1)$ when the tagging meson $B^0_{\rm tag}$ is a $B^0(\bar{B}^0)$, w is the average mistag probability, and Δw and μ describe the difference in mistag probability and the tagging efficiency asymmetry between B^0 and $\bar{B}^0$ mesons, respectively. The time distribution of the combinatorial background is assumed to have zero lifetime.

The Δt resolution function $\mathcal{R}$ is the sum of three Gaussian functions representing the core, tail, and outer part of the distribution, weighted by the Δt error for the core and the tail:

$$\mathcal{R}(\Delta t, \sigma_{\Delta t}) = f_{\rm core} G(\Delta t, \nu_{\rm core}\sigma_{\Delta t}, \sigma_{\rm core}\sigma_{\Delta t}) + f_{\rm tail} G(\Delta t, \nu_{\rm tail}\sigma_{\Delta t}, \sigma_{\rm tail}\sigma_{\Delta t}) + f_{\rm out} G(\Delta t, \nu_{\rm out}, \sigma_{\rm out}), \quad (62)$$

where $G(\Delta t, \sigma_{\Delta t}; \nu, \sigma)$ is a Gaussian distribution with mean ν and standard deviation σ, and f is the corresponding fraction. We have verified in simulation that the parameters of the resolution function for signal events are compatible with those obtained from the $B_{\rm flav}$ sample, a data sample of fully reconstructed $B^0 \to D^{(*)-}\pi^+/\rho^+/a_1^+$ decays. Therefore we use the $B_{\rm flav}$ parameters for better precision. The background Δt distribution is parametrized by the CP-asymmetric PDF $f(\Delta t, c_{\rm tag}) = 1 \pm \mathcal{A}_{\rm bkgd}(c_{\rm tag})$, convolved with the resolution function. The parameters of the background Δt PDF are determined in the fit to data from sidebands in $m_{\rm ES}$.

The detailed description of the treatment of the S and C terms of different contributing amplitudes is given in Sec. II D. Equation (61) is applicable to the time evolution of each of the five components in the angular distribution, three longitudinal (S_{J0} and C_{J0} for $J = 0$, 1, and 2) and two transverse (S_{JT} and C_{JT} for $J = 1$ and 2). All five S_{J0} and S_{JT} parameters are expressed in terms of $\Delta\phi_{00}$ and the other polarization and CP parameters entering the $\overset{(-)}{B}{}^0 \to \varphi K^{\pm}\pi^{\mp}$ PDF description, while the five C_{J0} and C_{JT} parameters are expressed through other polarization and CP parameters only, as shown in Eqs. (46)–(54).

For the combinatorial background we establish the functional forms and initial parameter values of the PDFs with data from sidebands in $m_{\rm ES}$ or ΔE. We then refine the main background parameters (excluding the resonance-mass central values and widths) by allowing them to vary in the final fit so that they are determined by the full data sample. Overall, there are 51 free background parameters in the joint fit.

C. Analysis validation

We validate the analysis selection and fit performance with a number of cross-check analyses. To test the treatment of combinatorial background in the PDF, we perform fits on the data collected below the $\Upsilon(4S)$ resonance, on GEANT-based [33] MC simulation of about 3 times the statistics of the data sample for both $q\bar{q}$ production (continuum) and generic $\Upsilon(4S) \to B\bar{B}$ decays. We also test the contribution of several dozen exclusive B meson decays which could potentially mimic the signal with statistics of more than an order of magnitude greater than their expectation. No significant bias in the background treatment was found. Systematic uncertainties associated with this treatment are discussed in the next subsection.

To test the signal PDF parametrization and the overall fit performance, we generate a large number of MC experiments, each one representing a statistically independent modeling of the fit to the data. The signal events are taken from the generated MC samples, while the background is generated from the PDF with the total sample size corresponding to the on-resonance data sample. We embed signal-like events according to expectation. We find the results of the MC experiments to be in good agreement with the expectations and the error estimates to be correct. In Fig. 7 we show examples of the $(x^{\rm fitted} - x^{\rm generated})/\sigma(x)$ distributions, where x denotes one of the signal parameters. The means and widths of all of these distributions are within about 5% of the expected values of zero and one, which results in negligibly small uncertainty in the fit result.

At all analysis development steps we used a "blind" technique. Numerical values of all physics parameters $n_{{\rm sig}J}$, $\mathcal{A}_{CPJ}$, $\Delta\phi_{00}$, and $\vec{\zeta}$ were kept hidden until the analysis method and tools were decided, validated, and

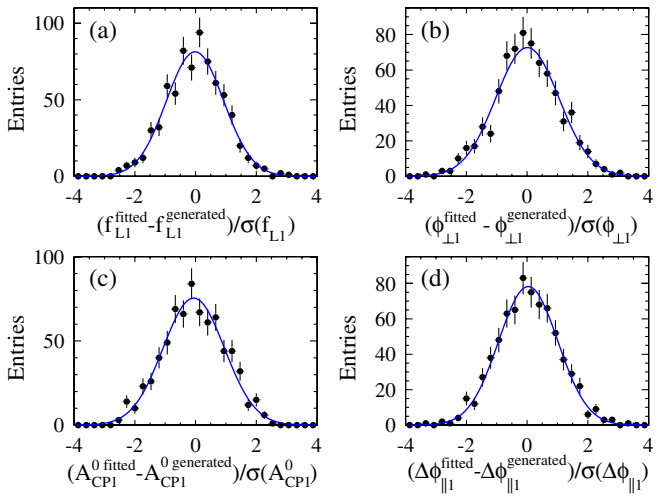

FIG. 7 (color online). Distributions of $(x^{\text{fitted}} - x^{\text{generated}})/\sigma(x)$ for a large number of generated MC experiments, where a Gaussian fit is superimposed, and x denotes signal parameters: (a) f_{L1}, (b) $\phi_{\perp 1}$, (c) A^0_{CP1}, and (d) $\Delta\phi_{\|1}$.

fixed. Consistency between the blind fit results and prediction from generated samples for the likelihood $\mathcal{L}$ and error values were used to judge the goodness of fit. We also examined the projection of data and likelihood fit PDFs onto individual variables with the enhancement of either signal or background to judge consistency. Detailed study of the systematic errors did not reveal any uncertainties which would exceed statistical errors.

D. Systematic uncertainties

In Tables VI, VII, and VIII we summarize the dominant sources of systematic errors in our measurements. In the measurement of the branching fractions, we tabulate separately the multiplicative errors on selection efficiency in Table VI. Measurement of all parameters suffers from uncertainties in the fit model which are discussed below and in Table VII. One additional error in the branching fraction measurement is the error on the number of $B^0\bar{B}^0$ mesons produced and is estimated to be 1.1%, where we assume equal decay rates of $\Upsilon(4S) \to B^0\bar{B}^0$ and B^+B^-. While most of the errors are dominated by uncertainties in the $\overset{(-)}{B}{}^0 \to \varphi K^\pm \pi^\mp$ decay mode, the measurement of $\Delta\phi_{00}$ has additional systematic errors unique to the $B^0 \to \varphi K^0_S \pi^0$ decay mode. Therefore all systematic errors on $\Delta\phi_{00}$ are quoted in Table VIII.

The systematic errors in the efficiency are typically due to imperfect MC simulation and they are obtained from independent studies, such as control samples. They affect the errors in the branching fraction but do not change the significance of the signal yield. From a study of absolute tracking efficiency, we evaluate the corrections to the track finding efficiencies, resulting in a systematic error of 0.5% per track and the total error of 2.0% for four tracks. The error due to particle identification is about 2% and is dominated by the kaon selection requirements. Particle identification performance has been validated with high-statistics data and MC control samples, such as $\bar{D}^*$-tagged $\bar{D} \to K\pi$ decays. The K^0_S selection efficiency systematic uncertainty is taken from an inclusive K^0_S control sample study, giving a total error of 3.5%. The π^0 reconstruction efficiency error is estimated to be 3.0% from a study of τ decays to modes with π^0 mesons.

The reconstruction efficiency has a weak dependence on the fraction of longitudinal polarization due to a nonuniform acceptance function of the helicity angles. Therefore, we use the measured value of the polarization when computing the efficiency. The uncertainty in this measurement translates into a systematic error in the branching fraction. Several requirements on the multihadronic final state,

TABLE VI. Systematic errors (%) in reconstruction efficiency evaluation. The total errors combine the two subchannels according to their weight and are dominated by the $K^\pm\pi^\mp$ channel. We separate the $\varphi(K\pi)^{*0}_0$ and $\varphi K^*_0(1430)^0$ modes to account for different errors in the daughter branching fractions. See text for details.

	$\varphi K^*(892)^0$		$\varphi K^*_2(1430)^0$		$\varphi(K\pi)^{*0}_0$		$\varphi K^*_0(1430)^0$	
	$K^\pm\pi^\mp$	$K^0_S\pi^0$	$K^\pm\pi^\mp$	$K^0_S\pi^0$	$K^\pm\pi^\mp$	$K^0_S\pi^0$	$K^\pm\pi^\mp$	$K^0_S\pi^0$
Track finding	2.0	1.0	2.0	1.0	2.0	1.0	2.0	1.0
PID	2.1	1.1	2.1	1.1	2.1	1.1	2.1	1.1
K^0_S selection	···	3.5	···	3.5	···	3.5	···	3.5
π^0 selection	···	3.0	···	3.0	···	3.0	···	3.0
MC statistics	0.2	0.3	0.2	0.3	0.3	0.4	0.3	0.4
Polarization	0.2	1.1	0.2	1.7	···	···	···	···
Event selection	1.0		1.0		1.0		1.0	
Thrust angle θ_T	1.0		1.0		1.0		1.0	
Vertex requirement	2.0		2.0		2.0		2.0	
φ branching fraction	1.2		1.2		1.2		1.2	
K^* branching fraction	0.0		2.4		0.0		10.8	
K^0_S branching fraction	···	0.1	···	0.1	···	0.1	···	0.1
Total	4.0		4.7		4.0		11.5	

TABLE VII. Systematic errors in the measurement of the three signal yields (%) and other signal parameters (absolute values), excluding the $\Delta\phi_{00}$ measurement. Uncertainties due to parametrization, acceptance function modeling, B-background (B-bkgd), fit response, interference of the $(K\bar{K})$ final states (interf.), charge asymmetry in reconstruction, assumptions about the unconstrained CP asymmetries $\mathcal{A}_{CP2}^{\perp}$ and $\Delta\phi_{\perp 2}$ (CP asym.), and the total errors are quoted. The errors are not quoted if they are either small or not relevant for a particular measurement. See text for details.

	PDF	Acceptance	B-bkgd	Fit	Interf.	Charge	CP asym.	Total
$\varphi(K\pi)_0^{*0}$ yield (%)	7.1	...	3.4	2.7	...	...	...	8.3
$\varphi K^*(892)^0$ yield (%)	2.3	...	1.9	1.3	1.8	...	...	3.7
$\varphi K_2^*(1430)^0$ yield (%)	3.3	...	0.8	2.8	...	...	...	4.4
$\mathcal{A}_{CP0}$	0.036	0.002	0.048	0.001	...	0.020	0.008	0.064
f_{L1}	0.002	0.002	0.005	0.007	0.010	...	...	0.013
$f_{\perp 1}$	0.001	0.001	0.006	0.004	0.010	...	...	0.013
$\phi_{\parallel 1}$	0.007	0.001	0.010	0.017	0.078	...	...	0.081
$\phi_{\perp 1}$	0.005	0.001	0.010	0.010	0.084	...	...	0.085
$\mathcal{A}_{CP1}$	0.007	0.001	0.008	0.012	0.018	0.020	...	0.031
$\mathcal{A}_{CP1}^{0}$	0.003	0.003	0.013	0.005	0.019	...	...	0.024
$\mathcal{A}_{CP1}^{\perp}$	0.007	0.004	0.022	0.024	0.052	...	...	0.062
$\Delta\phi_{\parallel 1}$	0.008	0.001	0.009	0.010	0.078	...	...	0.080
$\Delta\phi_{\perp 1}$	0.007	0.001	0.007	0.016	0.081	...	...	0.083
δ_{01}	0.030	0.001	0.005	0.003	0.080	...	...	0.086
$\Delta\delta_{01}$	0.008	0.001	0.006	0.006	0.080	...	...	0.081
f_{L2}	0.006	0.001	0.016	0.033	...	...	0.004	0.037
$f_{\perp 2}$	0.001	0.001	0.004	0.031	...	...	0.003	0.031
$\phi_{\parallel 2}$	0.051	0.002	0.021	0.029	...	...	0.012	0.063
$\mathcal{A}_{CP2}$	0.037	0.002	0.029	0.001	...	0.020	0.005	0.051
$\mathcal{A}_{CP2}^{0}$	0.012	0.001	0.005	0.002	...	...	0.003	0.014
$\Delta\phi_{\parallel 2}$	0.027	0.002	0.088	0.012	...	...	0.011	0.093
δ_{02}	0.117	0.004	0.062	0.009	...	...	0.006	0.133
$\Delta\delta_{02}$	0.012	0.004	0.057	0.009	...	...	0.007	0.059

minimum number of charged tracks, event shape, and vertex requirements result in a few percent errors. Other errors come from the uncertainty in the daughter branching fractions for $\varphi \to K^+K^-$ and $K^* \to K\pi$. All of these errors are summarized in Table VI.

TABLE VIII. Systematic errors (absolute values) in the measurement of $\Delta\phi_{00}$. See Table VII and text for details.

τ_B, Δm_B	0.001
sin2β measurement	0.015
Signal Δt resolution	0.016
Mistag differences	0.019
z scale + boost	0.002
Beam spot	0.010
SVT alignment	0.001
Tag-side interference	0.002
Background resolution and asymmetry	0.006
B-background	0.024
PDF	0.009
Acceptance	0.004
Fit	0.002
CP asym.	0.003
Total	0.041

When we perform the ML fit we make certain assumptions about the signal and background distributions. Most background parameters are allowed to vary in the fit, but we constrain most B decay parameters to the expectations based on MC and control samples. In order to account for the resulting uncertainty, we vary the parameters within their errors, taking into account correlations among the parameters. We obtain $m_{\rm ES}$, ΔE, and $\mathcal{F}$ uncertainties from the control samples discussed in Sec. III. The invariant mass uncertainties incorporate errors on the resonance parameters as quoted in Table IV and Ref. [18]. We take into account resolution in the $K\pi$ and K^+K^- invariant masses with the corresponding errors on the absolute values of 1 and 0.3 MeV, respectively.

We separate a special class of PDF uncertainties for the helicity angles, due to the acceptance function. In addition to statistical errors in the MC sample, we consider the momentum-dependent uncertainty of the tracking efficiency. The main effect is on the curvature of the acceptance function shown in Fig. 6 due to a strong correlation between the momentum of a track and the value of the helicity angle. Moreover, in order to study the effects of charge asymmetry in angular distributions, we apply the acceptance correction independently to only B or only $\bar{B}$

decay subsamples. The largest deviation is taken as the ''acceptance'' systematic error quoted in Table VII.

To estimate the effect of the B meson decays which could mimic signal, we study a full GEANT4-based MC simulation of the $\Upsilon(4S) \to B\bar{B}$ events. We embed the categories of events which may have ΔE and $m_{\rm ES}$ distributions similar to the signal into the data sample and observe variations of the fit results which we take as systematic errors. The nonresonant contribution is taken into account naturally in the fit with both $K\bar{K}$ and $K\pi$ contributions allowed to vary. The former is modeled as $B^0 \to f_0 K^{*0}$ and the latter is a part of the S-wave $K\pi$ parametrization. Interference effects are studied separately. We also take into account the uncertainty in the shape of the K^+K^- invariant mass distribution. The default parametrization assumes the $B^0 \to f_0 K^*(892)^0$ decay and we vary it to the phase-space $B^0 \to K^+K^-K^*(892)^0$ distribution. We constrain the number of $B^0 \to \varphi K^*(892)^0$ events contributing to the higher $K\pi$ invariant mass range based on the measured branching fraction, but we also vary this number according to the branching fraction errors. These errors are quoted as ''B-bkgd'' in Table VII.

The selected signal $B^0 \to \varphi K^{*0}$ events contain a small fraction of incorrectly reconstructed candidates. Misreconstruction occurs when at least one candidate track belongs to the decay products of the other B from the $\Upsilon(4S)$ decay, which happens in about 5% of the cases in the $\overset{(-)}{K}{}^{*0} \to K^\pm\pi^\mp$ decay. The distributions that show peaks for correctly reconstructed events have substantial tails, with large uncertainties in MC simulation, when misreconstructed events are included. These tails and incorrect angular dependence would reduce the power of the distributions to discriminate between the background and the collection of correctly and incorrectly reconstructed events. We choose, therefore, to represent only the correctly reconstructed candidates in the signal PDF and to calculate the reconstruction efficiency with both the correctly reconstructed and misreconstructed MC events. Fitting the generated samples to determine the number of correctly reconstructed candidates has an efficiency close to 100% even though a few percent of selected candidates are identified as background. We account for this with a systematic error taken as half of the fraction of candidates identified as background and quoted as the ''fit'' entry in Table VII. Similarly, we obtain systematic errors on other parameters from the largest deviation from the expectation. This includes a potential bias from the finite resolution in the helicity angle measurement and a possible dilution due to the presence of the misreconstructed component.

As we discuss below, a substantial $B^0 \to f_0 K\pi$ contribution is found in the lower $K\pi$ mass range, corresponding to either $B^0 \to f_0 K^*(892)^0$ decays or any other contribution with a broad K^+K^- invariant mass distribution, either resonant or nonresonant. The uncertainties due to $m_{K\bar{K}}$ interference are estimated with the samples generated according to the observed K^+K^- intensity and with various interference phases analogous to δ_{0J} in $K\pi$. These are the dominant systematic errors for the $\vec{\zeta}$ parameters of the $B^0 \to \varphi K^*(892)^0$ decay. No significant $B^0 \to f_0 K\pi$ contribution is observed in the higher $K\pi$ mass range.

The charge bias uncertainty affects only the relative yields of B and $\bar{B}$ events. We assign a systematic error of 2%, which accounts mostly for a possible asymmetry in the reconstruction of a charged kaon from a K^{*0} [39]. Overall charge asymmetry has a negligible effect on the angular asymmetry parameters, while the angular dependence of the charge asymmetry is tested with the flavor-dependent acceptance function discussed above.

There are still two CP parameters, $\mathcal{A}^\perp_{CP2}$ and $\Delta\phi_{\perp 2}$, that are not measured in the $\overset{(-)}{B}{}^0 \to \varphi \overset{(-)}{K}{}^*_2(1430)^0 \to \varphi K^\pm\pi^\mp$ decay. We assume zero asymmetry as the most likely value and vary them within ± 0.2 for the direct-CP asymmetry and ± 0.5 rad for the phase asymmetry. All of the errors on the fit parameters are summarized in Table VII.

For the time-dependent measurement of $\Delta\phi_{00}$, the variations are quoted in Table VIII. We vary the B^0 lifetime and Δm_B within their errors [18]. We include the error of the β measurement from Eq. (40). We use the results of the $\sin 2\beta$ analysis [34] to estimate the systematic errors related to signal parameters, such as Δt signal resolution and mistag differences, detector effects (z scale and boost, beam spot, SVT alignment uncertainties), and the tag-side interference. Background CP-asymmetry and resolution parameters are determined from the sideband data and then constrained in the fit. The constrained parameters are varied according to their errors and added in quadrature to compute the systematic errors.

V. RESULTS

We observe a nonzero yield with more than 10σ significance, including systematic uncertainties, in each of the three $B^0 \to \varphi K^{*0}$ decay modes. In Figs. 8–10 we show projections onto the discriminating variables. For illustration, the signal fraction is enhanced with a requirement on the signal-to-background probability ratio to be greater than a value within the range (0.85–0.95), calculated with the plotted variable excluded. This requirement is at least 50% efficient for the signal events.

In Tables IX and X the $n_{{\rm sig}J}$, $\mathcal{A}_{CPJ}$, $\Delta\phi_{00}$, and $\vec{\zeta} \equiv \{f_{LJ}, f_{\perp J}, \phi_{\|J}, \phi_{\perp J}, \delta_{0J}, \mathcal{A}^0_{CPJ}, \mathcal{A}^\perp_{CPJ}, \Delta\phi_{\|J}, \Delta\phi_{\perp J}, \Delta\delta_{0J}\}$ parameters of the $B^0 \to \varphi K^*(892)^0$, $\varphi K^*_2(1430)^0$, and $\varphi(K\pi)^{*0}_0$ decays are shown. The three quantities $\phi_{\perp 2}$, $\mathcal{A}^\perp_{CP2}$, and $\Delta\phi_{\perp 2}$, which characterize parity-odd transverse amplitude in the vector-tensor decay, are not measured because $f_{\perp 2}$ is found to be consistent with zero.

The computed significance of the yield is more than 24σ for $B^0 \to \varphi K^*(892)^0$ and 11σ for $B^0 \to \varphi(K\pi)^{*0}_0$. Given the convincing presence of the S-wave $(K\pi)^{*0}_0$ contribu-

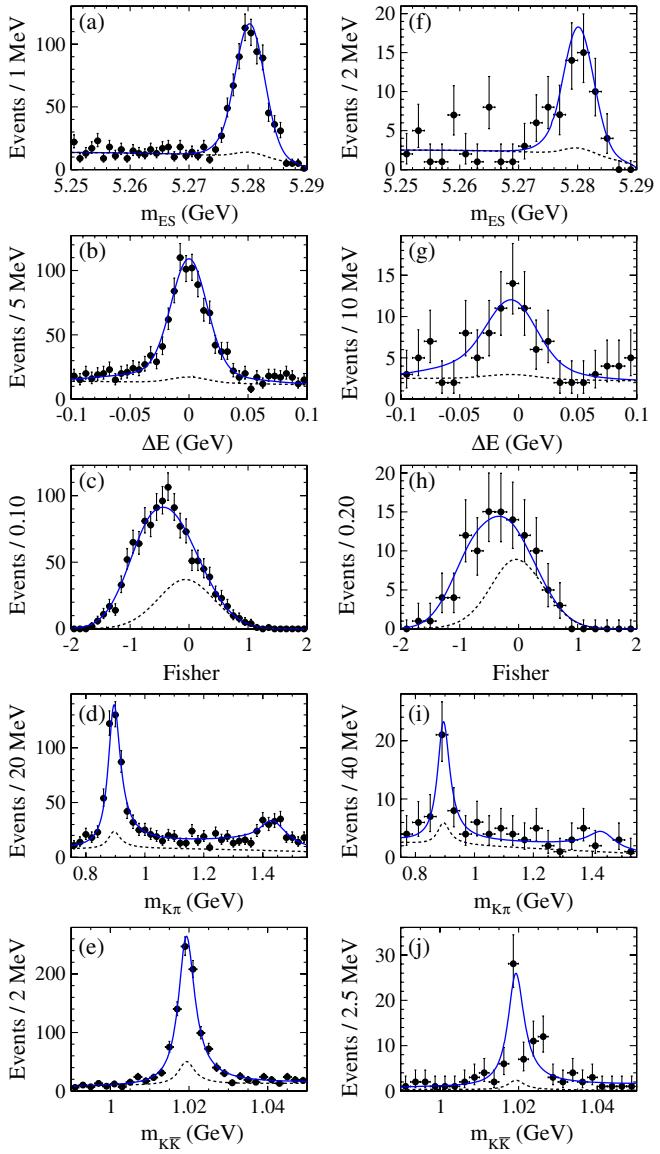

FIG. 8 (color online). Projections onto the variables $m_{\rm ES}$, ΔE, $\mathcal{F}$, $m_{K\pi}$, and $m_{K\bar{K}}$ for the signal $B \to \varphi K^{\pm}\pi^{\mp}$ (left) and $B \to \varphi K^0_S \pi^0$ (right) candidates. Data distributions are shown with a requirement on the signal-to-background probability ratio calculated with the plotted variable excluded. The solid (dashed) lines show the signal-plus-background (background) PDF projections.

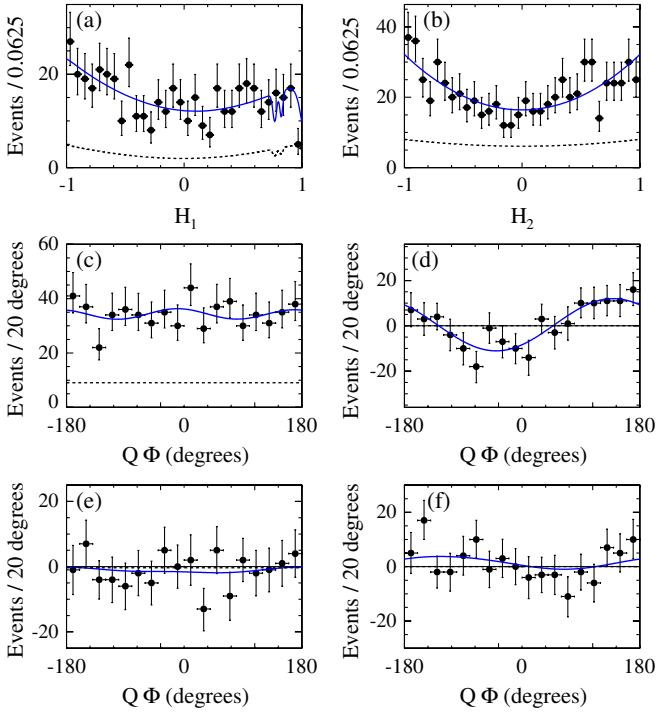

FIG. 9 (color online). Projections onto the variable $\mathcal{H}_1$ for the lower $m_{K\pi}$ range in (a) and $\mathcal{H}_2$ in (b). Projections onto $Q \times \Phi$ for the lower $m_{K\pi}$ range in (c)–(f) where Q changes sign between the B decays and the $\bar{B}$ decays. The distributions are shown for the signal $B^0 \to \varphi K^*(892)^0$ candidates following the solid (dashed) line definitions in Fig. 8. The Φ angle projections are shown for different combinations of event yields with certain requirements on the B flavor and $\mathcal{H}_1 \times \mathcal{H}_2$ product signs, as discussed in the text. The $D^{\pm}_{(s)}$-meson veto causes the sharp acceptance dips near $\mathcal{H}_1 = 0.8$ seen in (a).

tion, we rely on the interference terms to resolve the phase ambiguities. In the lower $m_{K\pi}$ range the yield of the $\varphi(K\pi)^{*0}_0$ contribution is 75^{+20}_{-17} events with a statistical significance of 9σ, including the interference term. From the measurements of the higher $m_{K\pi}$ range we calculate the contribution of $\varphi(K\pi)^{*0}_0$ to the lower mass range to be about 61 events. This is consistent with the above result within 1σ. The dependence of the interference on the $K\pi$ invariant mass [25,27] allows us to reject the other solution near $(2\pi - \phi_{\parallel 1}, \pi - \phi_{\perp 1})$ relative to that in Table X for the $B^0 \to \varphi K^*(892)^0$ decay with a statistical significance of 6.5σ (which becomes 5.4σ when systematic uncertainties are included). We also resolve this ambiguity with a statistical significance of more than 4σ with the $\bar{B}^0$ or B^0 decays independently. Figure 11 shows the $\chi^2 = -2\ln(\mathcal{L}/\mathcal{L}_{\rm max})$ scan plots for $\phi_{\parallel}$ and $\phi_{\perp}$, where we illustrate how the phase ambiguity is resolved. For comparison, we show the result of the fit where interference is not taken into account and no sensitivity to resolve the

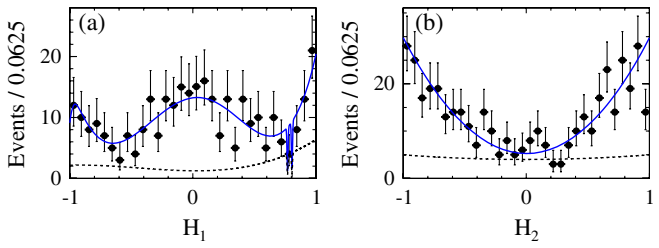

FIG. 10 (color online). Same as Figs. 9(a) and 9(b), but for the signal $B^0 \to \varphi K^*_2(1430)^0$ and $\varphi(K\pi)^{*0}_0$ candidates combined. The $D^{\pm}_{(s)}$-meson veto causes the sharp acceptance dips near $\mathcal{H}_1 = 0.8$ seen in (a).

TABLE IX. Analysis results: the reconstruction efficiency $\varepsilon_{\rm reco}$ obtained from MC simulation; the total efficiency ε, including the daughter branching fractions [18]; the number of signal events $n_{{\rm sig}J}$; statistical significance ($\mathcal{S}$) of the signal; the branching fraction $\mathcal{B}_J$; and the flavor asymmetry $\mathcal{A}_{CPJ}$. The branching fraction $\mathcal{B}(B^0 \to \varphi(K\pi)_0^{*0})$ refers to the coherent sum $|A_{\rm res} + A_{\rm nonres}|^2$ of resonant and nonresonant $J^P = 0^+$ $K\pi$ components and is quoted for $m_{K\pi} < 1.6$ GeV, while the $\mathcal{B}(B^0 \to \varphi K_0^*(1430)^0)$ is derived from it by integrating separately the B-W formula of the resonant $|A_{\rm res}|^2$ $K\pi$ component without $m_{K\pi}$ restriction. The systematic errors are quoted last.

Mode	$\varepsilon_{\rm reco}$ (%)	ε (%)	$n_{{\rm sig}J}$ (events)	$\mathcal{S}$ (σ)	$\mathcal{B}_J$ (10^{-6})	$\mathcal{A}_{CPJ}$
$\varphi K_0^*(1430)^0$					$3.9 \pm 0.5 \pm 0.6$	
$\varphi(K\pi)_0^{*0}$		8.3 ± 0.3	$172 \pm 24 \pm 14$	11	$4.3 \pm 0.6 \pm 0.4$	$+0.20 \pm 0.14 \pm 0.06$
$\to K^\pm\pi^\mp$	23.2 ± 0.9	7.6 ± 0.3	$158 \pm 22 \pm 13$			
$\to K_S^0\pi^0$	11.7 ± 0.4	0.66 ± 0.03	$14 \pm 2 \pm 1$			
$\varphi K^*(892)^0$		11.9 ± 0.4	$535 \pm 28 \pm 20$	24	$9.7 \pm 0.5 \pm 0.5$	$+0.01 \pm 0.06 \pm 0.03$
$\to K^\pm\pi^\mp$	33.7 ± 1.3	11.1 ± 0.4	$500 \pm 26 \pm 19$			
$\to K_S^0\pi^0$	13.8 ± 0.5	0.78 ± 0.03	$35 \pm 2 \pm 1$			
$\varphi K_2^*(1430)^0$		4.7 ± 0.2	$167 \pm 21 \pm 8$	11	$7.5 \pm 0.9 \pm 0.5$	$-0.08 \pm 0.12 \pm 0.05$
$\to K^\pm\pi^\mp$	26.7 ± 1.0	4.4 ± 0.2	$158 \pm 20 \pm 7$			
$\to K_S^0\pi^0$	8.7 ± 0.3	0.25 ± 0.01	$9 \pm 1 \pm 1$			

ambiguity is present. The significance of the deviations of $\phi_{\parallel 1}$ and $\phi_{\perp 1}$ from π is 5.4σ (4.5σ) and 6.1σ (5.0σ), respectively (including systematics in parentheses).

Projections onto $\mathcal{H}_1$ and $\mathcal{H}_2$ in the lower $m_{K\pi}$ range in Figs. 9(a) and 9(b) show sizable contributions of both $\cos^2\theta$ (longitudinal) and $\sin^2\theta$ (transverse) components. These two plots emphasize $f_{11}(\mathcal{H}_1, \mathcal{H}_2, \Phi)$ and $f_{21}(\mathcal{H}_1, \mathcal{H}_2, \Phi)$ angular terms in Eq. (8). Similarly, projections onto $\mathcal{H}_1$ and $\mathcal{H}_2$ in the higher $m_{K\pi}$ range in Fig. 10 show predominant longitudinal polarization with sizable $f_{12}(\mathcal{H}_1, \mathcal{H}_2, \Phi)$ and $f_{10}(\mathcal{H}_1, \mathcal{H}_2, \Phi)$ contributions, while the $f_{22}(\mathcal{H}_1, \mathcal{H}_2, \Phi)$ contribution is small.

In order to illustrate $f_{31}(\mathcal{H}_1, \mathcal{H}_2, \Phi)$ and $f_{41}(\mathcal{H}_1, \mathcal{H}_2, \Phi)$ angular distributions, we project onto the angle $-\Phi$ for the B decays and Φ for $\bar{B}$ decays. This procedure takes into account the change of sign for the odd components with P-wave amplitude ($A_{1\perp}$). This Φ angle projection is sensitive only to the constant term and to $\cos(2\Phi)$ and $\sin(2\Phi)$ terms. The fact that the double sine and cosine contributions are small in Fig. 9(c) tells us that both $(|A_{1\parallel}|^2 - |A_{1\perp}|^2)$ and $\Im m(A_{1\perp}A_{1\parallel}^*)$ are relatively small, in agreement with the fit results. That is, the values of $(1 - f_{L1} - 2f_{\perp 1})$ and $(\phi_{\parallel 1} - \phi_{\perp 1})$ are small; see α_{3J}^- and α_{4J}^- in Eqs. (11) and (12).

In order to emphasize $f_{51}(\mathcal{H}_1, \mathcal{H}_2, \Phi)$ and $f_{61}(\mathcal{H}_1, \mathcal{H}_2, \Phi)$ angular terms in Eq. (8), or $\cos\Phi$ and $\sin\Phi$ distributions, we show the difference between the above Φ angle projections for events with $\mathcal{H}_1 \times \mathcal{H}_2 > 0$ and with $\mathcal{H}_1 \times \mathcal{H}_2 < 0$. This gives us contributions to α_{5J}^- and α_{6J}^- in Eqs. (13) and (14), while background and all other signal contributions cancel. This projection is shown in Fig. 9(d), where we see good agreement between

TABLE X. Summary of the results; see Table II for definition of the parameters. The branching fractions $\mathcal{B}_J$ and flavor asymmetries $\mathcal{A}_{CPJ}$ are quoted from Table IX. The systematic errors are quoted last. The dominant fit correlation coefficients (ρ) are presented for the $\varphi K^*(892)^0$ and $\varphi K_2^*(1430)^0$ modes where we show correlations of δ_0 with $\phi_\parallel/\phi_\perp$ and of $\Delta\delta_0$ with $\Delta\phi_\parallel/\Delta\phi_\perp$.

Parameter	$\varphi K_0^*(1430)^0$ $J=0$	$\varphi K^*(892)^0$ $J=1$	ρ	$\varphi K_2^*(1430)^0$ $J=2$	ρ
$\mathcal{B}_J$ (10^{-6})	$3.9 \pm 0.5 \pm 0.6$	$9.7 \pm 0.5 \pm 0.5$		$7.5 \pm 0.9 \pm 0.5$	
f_{LJ}		$0.494 \pm 0.034 \pm 0.013$	$\}-48\%$	$0.901^{+0.046}_{-0.058} \pm 0.037$	$\}-15\%$
$f_{\perp J}$		$0.212 \pm 0.032 \pm 0.013$		$0.002^{+0.018}_{-0.002} \pm 0.031$	
$\phi_{\parallel J}$ (rad)		$2.40 \pm 0.13 \pm 0.08$	$\}+62\%$	$3.96 \pm 0.38 \pm 0.06$	$\cdots$
$\phi_{\perp J}$ (rad)		$2.35 \pm 0.13 \pm 0.09$		$\cdots$	
δ_{0J} (rad)		$2.82 \pm 0.15 \pm 0.09$	$+34\%/+25\%$	$3.41 \pm 0.13 \pm 0.13$	$+19\%$
$\mathcal{A}_{CPJ}$	$+0.20 \pm 0.14 \pm 0.06$	$+0.01 \pm 0.06 \pm 0.03$		$-0.08 \pm 0.12 \pm 0.05$	
$\mathcal{A}_{CPJ}^0$		$+0.01 \pm 0.07 \pm 0.02$	$\}-47\%$	$-0.05 \pm 0.06 \pm 0.01$	$\cdots$
$\mathcal{A}_{CPJ}^\perp$		$-0.04 \pm 0.15 \pm 0.06$		$\cdots$	
$\Delta\phi_{\parallel J}$ (rad)		$+0.22 \pm 0.12 \pm 0.08$	$\}+62\%$	$-1.00 \pm 0.38 \pm 0.09$	$\cdots$
$\Delta\phi_{\perp J}$ (rad)		$+0.21 \pm 0.13 \pm 0.08$		$\cdots$	
$\Delta\delta_{0J}$ (rad)		$+0.27 \pm 0.14 \pm 0.08$	$+35\%/+24\%$	$+0.11 \pm 0.13 \pm 0.06$	$+16\%$
$\Delta\phi_{00}$ (rad)	$0.28 \pm 0.42 \pm 0.04$				

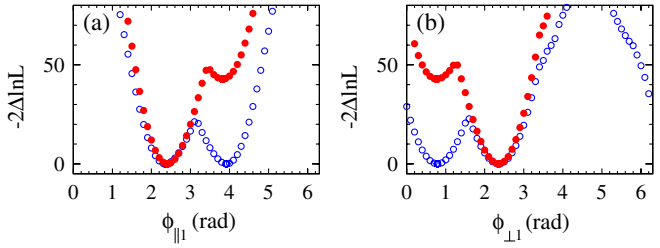

FIG. 11 (color online). Scan of $\chi^2 = -2\ln(\mathcal{L}/\mathcal{L}_{\max})$ as a function of $\phi_{\parallel 1}$ and $\phi_{\perp 1}$ for the $\varphi K^{\pm}\pi^{\mp}$ decays in the lower $m_{K\pi}$ range, where the solid circles are the results with the interference term, and the open circles without the interference term. Two discrete solutions are visible in the case without interference, while this ambiguity is resolved with the interference term. The values of $\Delta\phi_{\parallel 1}$ and $\Delta\phi_{\perp 1}$ have been constrained in the range $(-0.5, 0.5)$ in order to reject ambiguities with larger values of $\Delta\phi_{\parallel 1}$ and $\Delta\phi_{\perp 1}$.

the data and the fit results. This plot indicates a sizable cosΦ component due to $\Re e(A_{1\parallel}A_{10}^*)$ and an asymmetric sinΦ component due to $\Im m(A_{1\perp}A_{10}^*)$. The latter asymmetry is visible and reflects the presence of a strong phase with a statistical significance of 6.4σ.

In order to emphasize CP asymmetries in the angular distributions we make two other similar projections onto the Φ angle, but now we plot the difference between the B and $\bar{B}$ decays. Figures 9(e) and 9(f) show distributions of $(N_{B>} - N_{\bar{B}>} + N_{B<} - N_{\bar{B}<})$ and $(N_{B>} - N_{\bar{B}>} - N_{B<} + N_{\bar{B}<})$, where $N_{B>}$ denotes the number of B decays with $\mathcal{H}_1\mathcal{H}_2 > 0$, $N_{\bar{B}>}$ is the number of $\bar{B}$ decays with $\mathcal{H}_1\mathcal{H}_2 > 0$, $N_{B<}$ is the number of B decays with $\mathcal{H}_1\mathcal{H}_2 < 0$, and $N_{\bar{B}<}$ is the number of $\bar{B}$ decays with $\mathcal{H}_1\mathcal{H}_2 < 0$. In all cases we project onto $-\Phi$ for the B decays and onto Φ for the $\bar{B}$ decays. Figure 9(e) is sensitive to CP asymmetries in the cos(2Φ) and sin(2Φ) terms in Eqs. (11) and (12), while Fig. 9(f) is sensitive to CP asymmetries in the cosΦ and sinΦ terms in Eqs. (13) and (14). In particular, there is a hint of a sine wave contribution in Fig. 9(f), corresponding to the nonzero measurement of $\Delta\phi_{\perp 1} = +0.21 \pm 0.13 \pm 0.08$, though not significant enough to constitute evidence for CP violation.

In Table X we summarize the correlation among the primary fit parameters. There are two large correlation effects of approximately 50% evident for the $B^0 \to \varphi K^*(892)^0$ decay in the fit, that is, between the longitudinal and transverse fractions (f_{L1} and $f_{\perp 1}$) and between the two phases ($\phi_{\parallel 1}$ and $\phi_{\perp 1}$). In Fig. 12 we show the likelihood function contour plots for the above pairs of correlated observables as well as for f_{L2} and $f_{\perp 2}$. Figure 13 shows the $\chi^2 = -2\ln(\mathcal{L}/\mathcal{L}_{\max})$ distributions for the CP violation phase parameters $\Delta\delta_{xJ}$ and $\Delta\phi_{xJ}$, where x stands for either $\perp$, $\parallel$, or 0.

The $B^0 \to f_0 K^{*0}$ category accounts for final states with K^+K^- from either f_0, a_0, or any other broad K^+K^-

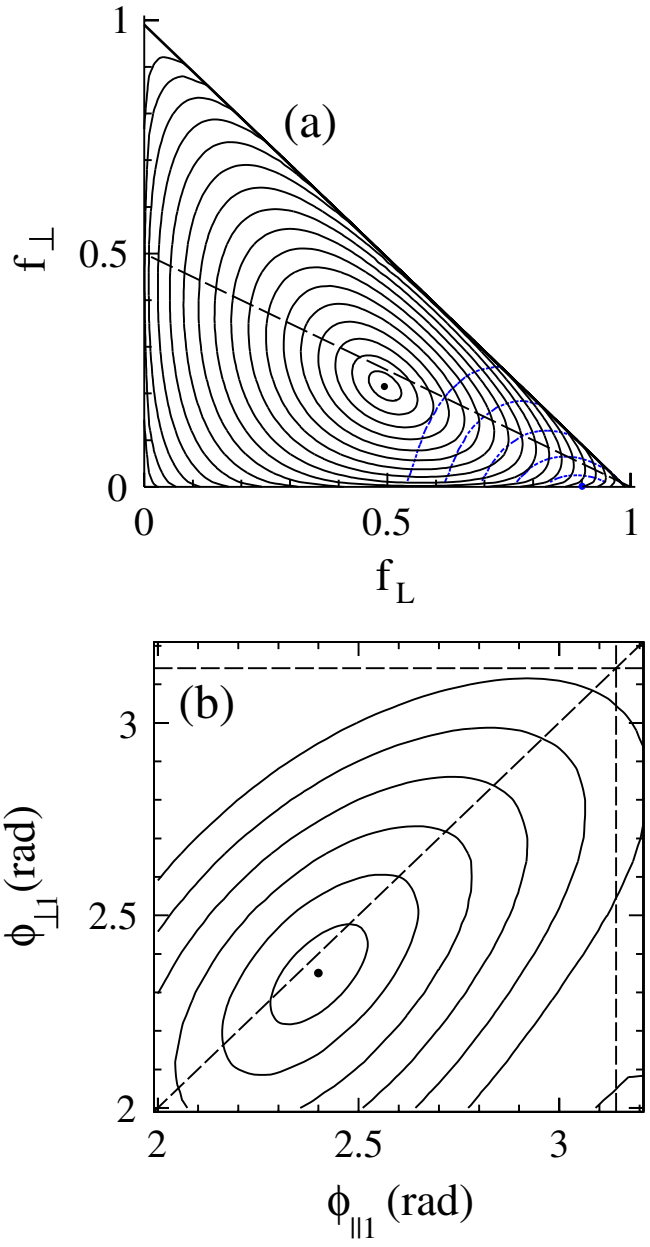

FIG. 12 (color online). Contours corresponding to the unit intervals of $\sqrt{-2\Delta\ln\mathcal{L}}$ for polarization $f_{\perp J}$ and f_{LJ} (a) and phase $\phi_{\perp 1}$ and $\phi_{\parallel 1}$ (b) measurements. Diagonal dashed lines $f_{\perp J} = (1 - f_{LJ})/2$ and $\phi_{\perp 1} = \phi_{\parallel 1}$ correspond to $|A_{J+1}| \gg |A_{J-1}|$. In (a), the solid (dashed) contours are the results for $J = 1$ ($J = 2$). In (b) the (π, π) point is indicated by the crossed dashed lines.

contribution under the φ. Its yield is consistent with zero in the higher $m_{K\pi}$ range and is 84 ± 19 events in the lower $m_{K\pi}$ range. Because of uncertainties in the nature of this contribution, we do not calculate its branching fraction but include it in the evaluation of systematic uncertainties in other parameters as discussed above.

In Fig. 14 we illustrate the effect of interference in the $K\pi$ invariant mass. In the vector-scalar $K\pi$ interference

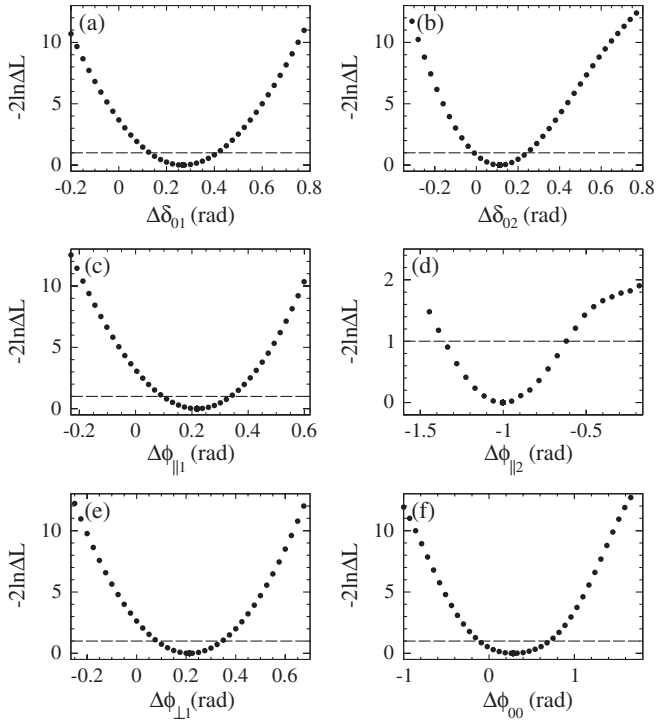

FIG. 13. Scan of $\chi^2 = -2\ln(\mathcal{L}/\mathcal{L}_{\max})$ as a function of (a) $\Delta\delta_{01}$, (b) $\Delta\delta_{02}$, (c) $\Delta\phi_{\|1}$, (d) $\Delta\phi_{\|2}$, (e) $\Delta\phi_{\perp 1}$, and (f) $\Delta\phi_{00}$.

(lower mass range) the interference term is linear in $\mathcal{H}_1$, creating a forward-backward asymmetry. However, due to variation of the B-W phase this effect cancels when integrated over the $m_{K\pi}$ range. For $\delta_0 \simeq \pi$ we expect the coefficient in front of $\mathcal{H}_1$ to be positive above $m_{K\pi} \simeq 0.896$ GeV and negative below this value. Thus, we create Fig. 14(a) to emphasize this effect. If $\delta_{01} \simeq 0$, the sign of the forward-backward asymmetry would be reversed and we would see more events on the left as opposed to the right. Thus $\delta_{01} \simeq \pi$ is preferred. We note that this plot has

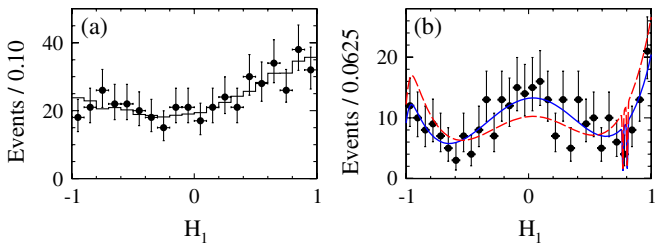

FIG. 14 (color online). Projections onto the variable $\pm\mathcal{H}_1$. (a) Low $m_{K\pi}$ mass range, where we project the data onto $\mathcal{H}_1$ for $m_{K\pi} > 0.896$ GeV and onto $-\mathcal{H}_1$ for $m_{K\pi} < 0.896$ GeV. The points with error bars show data and the histogram corresponds to the results of the MC generated with the observed polarization parameters. (b) High $m_{K\pi}$ mass range, where we project the data onto $\mathcal{H}_1$. Points with error bars represent the data, while the solid line represents the PDF projection with the interference term and the dashed line without the interference term included. The $D^{\pm}_{(s)}$-meson veto causes the sharp acceptance dips near $\mathcal{H}_1 = 0.8$.

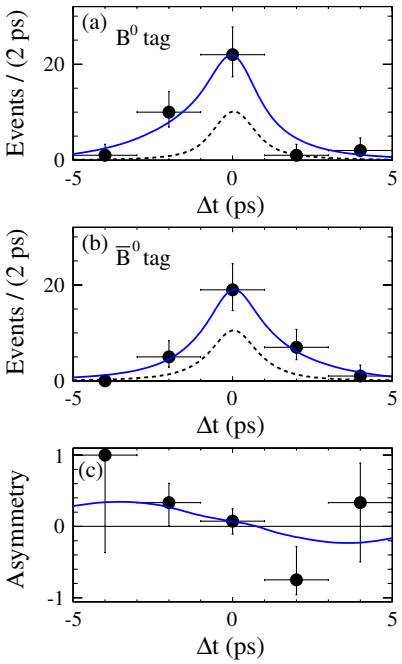

FIG. 15 (color online). The distribution of Δt for events in the signal region, for $B^0_{\rm tag}$ (a) and $\bar{B}^0_{\rm tag}$ (b) events with the fit result overlaid. The solid (dashed) lines show the signal-plus-background (background) PDF projections. The asymmetry $\mathcal{A}(\Delta t)$ shown in (c) is defined in Eq. (34).

only partial information about the interference while the multidimensional fit uses the full information to extract the result.

Figure 14(b) shows a similar effect in the tensor-scalar $K\pi$ interference (higher mass range). In this case interference could either enhance events in the middle of the $\mathcal{H}_1$ distribution and deplete them at the edges, or the other way around. Figure 14(b) indeed shows significant improvement in the $\mathcal{H}_1$ parametrization with the inclusion of interference. It also corresponds to the observed value $\delta_{02} \simeq \pi$.

Because of the low significance of our measurements of $f_{\|2} = (1 - f_{L2} - f_{\perp 2})$ (1.9σ) and $f_{\perp 2}$ (0σ) in the $B^0 \to \varphi K_2^*(1430)^0$ decay we have insufficient information to constrain $\phi_{\|2}$ at higher significance or to measure $\phi_{\perp 2}$, $A^{\perp}_{CP2}$, or $\Delta\phi_{\perp 2}$, which we constrain to zero in the fit.

Finally, we fit a single parameter $\Delta\phi_{00}$ in the time evolution after combining all available $B^0 \to \varphi K^0_S \pi^0$ charmless final states, which are dominated by spin-0, 1, and 2 $(K\pi)$ combinations. The distribution of the time difference Δt and the time-dependent asymmetry are shown in Fig. 15. The parameter $\Delta\phi_{00}$ is measured to be $0.28 \pm 0.42 \pm 0.04$, as shown in Table X.

VI. CONCLUSION

In conclusion, we have performed an amplitude analysis and searched for CP violation in the angular distribution of

$B^0 \to \varphi K^{*0}$ decays with tensor, vector, and scalar K^{*0} mesons. Our results are summarized in Tables IX and X and supersede corresponding measurements in Ref. [20]. In this analysis we employ several novel techniques for CP-violation and polarization measurements in the study of a single B-decay topology $B^0 \to \varphi(K\pi)$. We use the time evolution of the $B^0 \to \varphi K^0_S \pi^0$ channel to extract the CP-violating phase difference $\Delta\phi_{00} = 0.28 \pm 0.42 \pm 0.04$ between the B and $\bar{B}$ decay amplitudes. We use the dependence on the $K\pi$ invariant mass of the interference between the scalar and vector, or scalar and tensor components to resolve discrete ambiguities of both the strong and weak phases. Twelve parameters are measured for the vector-vector decay, nine parameters for the vector-tensor decay, and three parameters for the vector-scalar decay, including the branching fractions, CP-violation parameters, and parameters sensitive to final-state interactions.

The $(V\text{-}A)$ structure of the weak interaction and the s-quark spin-flip suppression in the process shown in Fig. 1 suggest $|A_{J0}| \gg |A_{J+1}| \gg |A_{J-1}|$ [13,16]. The relatively small value of $f_{L1} = 0.494 \pm 0.034 \pm 0.013$ and the relatively large value of $f_{\perp 1} = 0.212 \pm 0.032 \pm 0.013$ in the vector-vector decay remain a puzzle. The naive expectation is that the $V\text{-}A$ nature of the weak decays requires that an antiquark originating from the $\bar{b} \to \bar{q}W^+$ decay be produced in helicity state $+\frac{1}{2}$. This argument applies to the penguin loop which is a purely weak transition, $\bar{b} \to \bar{s}$, with the double-W coupling in the standard model. The $\bar{s}$ antiquark can couple to the s quark (see Fig. 1) to produce the φ state with helicity of either $\lambda = 0$ or $\lambda = +1$, but not $\lambda = -1$. However, the K^* state should have the same helicity as the φ due to angular momentum conservation. The $\lambda = +1$ state is not allowed in this case because both s and $\bar{s}$ quarks would have helicity $+\frac{1}{2}$, in violation of helicity conservation in the vector coupling $g \to s\bar{s}$.

The spin flip can alter both of the above requirements, but its suppression factor is of order $\sim m_V/m_B$ for each flip, where m_V is the mass of the φ or K^{*0} mesons. Thus, we arrive at the expectation $|A_{J0}| \gg |A_{J+1}| \gg |A_{J-1}|$, or $|A_{J0}| \gg |A_{J\perp}|$ and $A_{J\perp} \simeq A_{J\parallel}$, where A_{J+1} is suppressed by one spin flip, while A_{J-1} is suppressed by two spin flips. New physics could have different interactions, alter the spin-helicity expectations and result in a large fraction of transverse polarization. Alternatively, strong-interaction effects might change this expectation [16]. The value of $f_{L2} = 0.901^{+0.046}_{-0.058} \pm 0.037$ in vector-tensor decays is not compatible with that measured in vector-vector decays, while it is compatible with the expectation from the spin-flip analysis above. This points to a unique role for the spin-1 particle recoiling against the φ in the $B \to \varphi K^*$ polarization puzzle.

In the $B^0 \to \varphi K^*(892)^0$ decay we obtain the solution $\phi_{\parallel 1} \simeq \phi_{\perp 1}$ without discrete ambiguities. Combined with the approximate solution $f_{L1} \simeq 1/2$ and $f_{\perp 1} \simeq (1 - f_{L1})/2$, this results in the approximate decay amplitude hierarchy $|A_{10}| \simeq |A_{1+1}| \gg |A_{1-1}|$ (and $|\bar{A}_{10}| \simeq |\bar{A}_{1-1}| \gg |\bar{A}_{1+1}|$). We find more than 5σ (4σ) deviation, including systematic uncertainties, of $\phi_\perp(\phi_\parallel)$ from either π or zero in the $B^0 \to \varphi K^*(892)^0$ decay, indicating the presence of final-state interactions (FSI) not accounted for in the naive factorization. The effect of FSI is evident in the phase shift of the cosine distribution in Fig. 9(d).

From the definition in Eq. (46) and the measurement of $\Delta\phi_{00}$, we determine the parameter

$$\sin(2\beta_{\rm eff}) = \sin(2\beta + 2\Delta\phi_{00}) = 0.97^{+0.03}_{-0.52}, \qquad (63)$$

as measured with the $B^0 \to \varphi K^*_0(1430)^0$ decay. Our measurements of eleven CP-violation parameters rule out a significant part of the physical region and are consistent with no CP violation in the direct decay, but are consistent with the measurement of $\sin(2\beta_{\rm eff})$ in Eq. (63). The current precision on $\sin(2\beta_{\rm eff})$ is still statistics-limited, although we constrain $\sin(2\beta_{\rm eff}) > 0.15$ at the 90% confidence level, which is consistent with the standard model CP violation due to B^0-$\bar{B}^0$ mixing. This analysis provides techniques for future experiments to extract this parameter from the $B^0 \to \varphi K\pi$ decays.

Other significant nonzero CP-violation parameters would indicate the presence of new amplitudes with different weak phases. The parameters $\Delta\phi_{\perp J}$ and $\Delta\phi_{\parallel J}$ are particularly interesting due to their sensitivity to the weak phases of the amplitudes without hadronic uncertainties [17], such as the relative weak phases of A_{J+1} and A_{J0}, while the CP-violation parameter $\Delta\delta_{0J}$ represents potential differences of weak phases among decay modes.

We note that the measurement of $\sin(2\beta_{\rm eff})$ in Eq. (63) is not the primary result of this analysis but only an interpretation of the $\Delta\phi_{00}$ measurement. Equivalently, there could be six other effective $\sin(2\beta)$ measurements as shown in Eqs. (47)–(49). However, all of them would be highly correlated due to the same dominant uncertainty coming from $\Delta\phi_{00}$. Rather than give them all here, we provide an illustration of our measurements with the following differences using the results in Table X as input:

$$\sin(2\beta - 2\Delta\delta_{01}) - \sin(2\beta) = -0.42^{+0.26}_{-0.34}, \qquad (64)$$

$$\sin(2\beta - 2\Delta\phi_{\parallel 1}) - \sin(2\beta) = -0.32^{+0.22}_{-0.30}, \qquad (65)$$

$$\sin(2\beta - 2\Delta\phi_{\perp 1}) - \sin(2\beta) = -0.30^{+0.23}_{-0.32}, \qquad (66)$$

$$\sin(2\beta - 2\Delta\phi_{\perp 1}) - \sin(2\beta - 2\Delta\phi_{\parallel 1}) = 0.02 \pm 0.23, \qquad (67)$$

$$\sin(2\beta - 2\Delta\delta_{02}) - \sin(2\beta) = -0.10^{+0.18}_{-0.29}. \qquad (68)$$

Systematic uncertainties are included in the errors quoted in Eqs. (63)–(68).

Taking the example in Eq. (67), we see that because of the positive correlation between $\Delta\phi_{\perp 1}$ and $\Delta\phi_{\parallel 1}$, we

achieve a precision of ± 0.23 on the measurement of the difference between values of $\sin(2\beta_{\rm eff})$ from the parity-odd ($A_{1\perp}$) and parity-even ($A_{1\|}$) decay amplitudes. This precision is significantly better than that of the measurement of $\sin(2\beta_{\rm eff})$ itself because of the cancellation of common uncertainties. A significant deviation from zero would indicate a *CP*-violating contribution to either the parity-odd or parity-even amplitude but not the other. A similar comparison would be the values of $\sin(2\beta_{\rm eff})$ measured in $B \to \eta' K$ and $B \to \varphi K$ decays. This measurement of the $\sin(2\beta_{\rm eff})$ difference with the parity-odd and parity-even amplitudes is possible with the angular analysis alone without any time-dependent measurement.

Among other results in this analysis, we note the significant yield of events (more than 5σ statistical significance) in the category $B^0 \to (K^+K^-)K^*(892)^0$, where (K^+K^-) reflects an *S*-wave contribution, which could be an f_0 or a_0 meson, or any other scalar component. This decay is of the scalar-vector type. We have already observed such decays with $B^0 \to \varphi K_0^*(1430)^0$, as discussed in this paper. Therefore it is plausible that the two decays are related by SU(3) symmetry. However, we do not report the branching fraction of $B^0 \to (K^+K^-)K^*(892)^0$ because the exact nature of the process is not known, and a more detailed study together with $B^0 \to (\pi^+\pi^-)K^*(892)^0$ is required. Nonetheless, interference between the $B^0 \to (K^+K^-)K^*(892)^0$ and $B^0 \to \varphi K^*(892)^0$ decays provides a further path for relating strong and weak phases in the two processes, similar to the interference studies presented in this analysis. At present this interference is considered in the study of systematic uncertainties with good prospects for phase measurements from higher statistics experiments.

ACKNOWLEDGMENTS

We are grateful for the extraordinary contributions of our PEP-II colleagues in achieving the excellent luminosity and machine conditions that have made this work possible. The success of this project also relies critically on the expertise and dedication of the computing organizations that support *BABAR*. The collaborating institutions wish to thank SLAC for its support and the kind hospitality extended to them. This work is supported by the U.S. Department of Energy and National Science Foundation, the Natural Sciences and Engineering Research Council (Canada), the Commissariat à l'Energie Atomique and Institut National de Physique Nucléaire et de Physique des Particules (France), the Bundesministerium für Bildung und Forschung and Deutsche Forschungsgemeinschaft (Germany), the Istituto Nazionale di Fisica Nucleare (Italy), the Foundation for Fundamental Research on Matter (The Netherlands), the Research Council of Norway, the Ministry of Education and Science of the Russian Federation, Ministerio de Educación y Ciencia (Spain), and the Science and Technology Facilities Council (United Kingdom). Individuals have received support from the Marie-Curie IEF program (European Union) and the A. P. Sloan Foundation.

[1] A. D. Sakharov, Pis'ma Zh. Eksp. Teor. Fiz. **5**, 32 (1967) [JETP Lett. **5**, 24 (1967)].
[2] J. H. Christenson, J. Cronin, V. Fitch, and R. Turlay, Phys. Rev. Lett. **13**, 138 (1964).
[3] B. Aubert *et al.* (*BABAR* Collaboration), Phys. Rev. Lett. **87**, 091801 (2001); K. Abe *et al.* (Belle Collaboration), Phys. Rev. Lett. **87**, 091802 (2001); B. Aubert *et al.* (*BABAR* Collaboration), Phys. Rev. Lett. **99**, 171803 (2007); K.-F. Chen *et al.* (Belle Collaboration), Phys. Rev. Lett. **98**, 031802 (2007).
[4] A. Alavi-Harati *et al.* (KTeV Collaboration), Phys. Rev. Lett. **83**, 22 (1999); V. Fanti *et al.* (NA48 Collaboration), Phys. Lett. B **465**, 335 (1999); G. D. Barr *et al.* (NA31 Collaboration), Phys. Lett. B **317**, 233 (1993).
[5] B. Aubert *et al.* (*BABAR* Collaboration), Phys. Rev. Lett. **93**, 131801 (2004); Y. Chao *et al.* (Belle Collaboration), Phys. Rev. Lett. **93**, 191802 (2004); B. Aubert *et al.* (*BABAR* Collaboration), Phys. Rev. Lett. **99**, 021603 (2007).
[6] M. Bander, D. Silverman, and A. Soni, Phys. Rev. Lett. **43**, 242 (1979).
[7] M. Kobayashi and T. Maskawa, Prog. Theor. Phys. **49**, 652 (1973); N. Cabibbo, Phys. Rev. Lett. **10**, 531 (1963).
[8] For a review, see S. Weinberg, *The Quantum Theory of Fields* (Cambridge University Press, Cambridge, 1999), Vol. 3.
[9] B. H. Behrens *et al.* (CLEO Collaboration), Phys. Rev. Lett. **80**, 3710 (1998).
[10] R. A. Briere *et al.* (CLEO Collaboration), Phys. Rev. Lett. **86**, 3718 (2001); B. Aubert *et al.* (*BABAR* Collaboration), Phys. Rev. Lett. **87**, 151801 (2001).
[11] B. Aubert *et al.* (*BABAR* Collaboration), Phys. Rev. Lett. **98**, 031801 (2007).
[12] L. Silvestrini, Annu. Rev. Nucl. Part. Sci. **57**, 405 (2007).
[13] A. Ali *et al.*, Z. Phys. C **1**, 269 (1979); G. Valencia, Phys. Rev. D **39**, 3339 (1989); G. Kramer and W. F. Palmer, Phys. Rev. D **45**, 193 (1992); H.-Y. Cheng and K.-C. Yang, Phys. Lett. B **511**, 40 (2001); C.-H. Chen *et al.*, Phys. Rev. D **66**, 054013 (2002); M. Suzuki, Phys. Rev. D **66**, 054018 (2002); A. Datta and D. London, Int. J. Mod. Phys. A **19**, 2505 (2004).

[14] B. Aubert *et al.* (*BABAR* Collaboration), Phys. Rev. Lett. **91**, 171802 (2003); **93**, 231804 (2004); arXiv:hep-ex/0303020.
[15] K.-F. Chen *et al.* (Belle Collaboration), Phys. Rev. Lett. **91**, 201801 (2003); **94**, 221804 (2005).
[16] A. L. Kagan, Phys. Lett. B **601**, 151 (2004); Y. Grossman, Int. J. Mod. Phys. A **19**, 907 (2004); C. W. Bauer *et al.*, Phys. Rev. D **70**, 054015 (2004); P. Colangelo *et al.*, Phys. Lett. B **597**, 291 (2004); M. Ladisa *et al.*, Phys. Rev. D **70**, 114025 (2004); E. Alvarez *et al.*, Phys. Rev. D **70**, 115014 (2004); H. Y. Cheng *et al.*, Phys. Rev. D **71**, 014030 (2005); H. n. Li and S. Mishima, Phys. Rev. D **71**, 054025 (2005); P. K. Das and K. C. Yang, Phys. Rev. D **71**, 094002 (2005); C. H. Chen and C. Q. Geng, Phys. Rev. D **71**, 115004 (2005); Y. D. Yang *et al.*, Phys. Rev. D **72**, 015009 (2005); K. C. Yang, Phys. Rev. D **72**, 034009 (2005); C. S. Huang *et al.*, Phys. Rev. D **73**, 034026 (2006); M. Beneke *et al.*, Phys. Rev. Lett. **96**, 141801 (2006); C. H. Chen and H. Hatanaka, Phys. Rev. D **73**, 075003 (2006); M. Beneke *et al.*, Nucl. Phys. **B774**, 64 (2007); C.-H. Chen and C.-Q. Geng, Phys. Rev. D **75**, 054010 (2007); A. Datta *et al.*, Phys. Rev. D **76**, 034015 (2007); **77**, 114025 (2008); H.-Y. Cheng and K.-C. Yang, arXiv:0805.0329.
[17] A. V. Gritsan and J. G. Smith, review in [18], Phys. Lett. B **667**, 910 (2008).
[18] C. Amsler *et al.* (Particle Data Group), Phys. Lett. B **667**, 1 (2008).
[19] B. Aubert *et al.* (*BABAR* Collaboration), Phys. Rev. D **69**, 011102 (2004).
[20] B. Aubert *et al.* (*BABAR* Collaboration), Phys. Rev. Lett. **98**, 051801 (2007).
[21] B. Aubert *et al.* (*BABAR* Collaboration), Phys. Rev. Lett. **101**, 161801 (2008).
[22] B. Aubert *et al.* (*BABAR* Collaboration), Phys. Rev. Lett. **99**, 201802 (2007).
[23] B. Aubert *et al.* (*BABAR* Collaboration), Phys. Rev. D **76**, 051103(R) (2007).
[24] J. Zhang *et al.* (Belle Collaboration), Phys. Rev. Lett. **95**, 141801 (2005); B. Aubert *et al.* (*BABAR* Collaboration), Phys. Rev. Lett. **97**, 201801 (2006).
[25] D. Aston *et al.* (LASS Collaboration), Nucl. Phys. **B296**, 493 (1988).
[26] W. M. Dunwoodie, on behalf of the LASS Collaboration (private communication).
[27] B. Aubert *et al.* (*BABAR* Collaboration), Phys. Rev. D **71**, 032005 (2005); B. Aubert *et al.* (*BABAR* Collaboration), Phys. Rev. D **78**, 012004 (2008).
[28] E. P. Wigner, Phys. Rev. **98**, 145 (1955).
[29] The *BABAR* Physics Book, SLAC Report No. SLAC-R-504, edited by P. Harrison and H. Quinn (Stanford Linear Accelerator Center, Menlo Park, CA, 1998).
[30] B. Aubert *et al.* (*BABAR* Collaboration), Phys. Rev. Lett. **99**, 161802 (2007).
[31] I. Dunietz *et al.*, Phys. Rev. D **43**, 2193 (1991).
[32] B. Aubert *et al.* (*BABAR* Collaboration), Nucl. Instrum. Methods Phys. Res., Sect. A **479**, 1 (2002).
[33] S. Agostinelli *et al.* (GEANT4 Collaboration), Nucl. Instrum. Methods Phys. Res., Sect. A **506**, 250 (2003).
[34] B. Aubert *et al.* (*BABAR* Collaboration), Phys. Rev. Lett. **99**, 171803 (2007).
[35] F. James *et al.*, MINUIT, Function Minimization and Error Analysis CERN Program Library.
[36] R. Brun and F. Rademakers, Nucl. Instrum. Methods Phys. Res., Sect. A **389**, 81 (1997); see also http://root.cern.ch/.
[37] H. Albrecht *et al.* (ARGUS Collaboration), Phys. Lett. B **241**, 278 (1990).
[38] E. M. Aitala *et al.* (E791 Collaboration), Phys. Rev. Lett. **86**, 765 (2001).
[39] B. Aubert *et al.* (*BABAR* Collaboration), Phys. Rev. D **65**, 051101 (2002).